https://doi.org/10.5194/egusphere-2025-6294
Preprint. Discussion started: 12 January 2026

Groundwater Hysteresis Increasingly Decouples Flowing Network Length from Streamflow as Snow Shifts to Rain

Elijah N. Boardman[1,2], Mark S. Wigmosta[3], Nicole M. Fernandez[4], John A. Whiting[1], Adrian A. Harpold[1,5]

[1]Mountain Hydrology LLC, Reno, Nevada, 89503, USA
[2]Graduate Program of Hydrologic Sciences, University of Nevada, Reno, Reno, Nevada, 89557, USA
[3]Energy and Environment Directorate, Pacific Northwest National Laboratory, Richland, WA, 99354, USA
[4]Department of Earth and Planetary Sciences, ETH Zürich, 8092 Zürich, Switzerland
[5]Department of Natural Resources and Environmental Science, University of Nevada, Reno, Reno, Nevada, 89557, USA

Correspondence to: Elijah N. Boardman (eli.boardman@mountainhydrology.com)

Abstract. Flowing stream networks expand and contract in response to dynamic groundwater levels. Field studies generally associate greater flowing network length (L) with higher streamflow (Q), but this neglects potential hysteresis caused by nonequilibrium groundwater flow after rain and snowmelt. Using a new version of the Distributed Hydrology Soil Vegetation Model (DHSVM), we hypothesize that groundwater hysteresis may decouple L from Q across large (>100%) variations in Q. In a 27 km^2 snowy volcanic watershed, seasonal anomalies in measured stream ionic concentration indicate an outsized contribution from longer subsurface flowpaths during recession, supporting our L-Q hysteresis hypothesis and refining our model calibration. The model can reproduce observed stream network elasticity (from field surveys), and the predicted network length anomaly mirrors seasonal anomalies in measured stream ionic concentration ($r = -0.92$), suggesting that the model can capture the seasonal reconfiguration of groundwater flowpaths. A warmer climate is expected to cause a partial transition from snow to rain resulting in flashier streamflow, but our simulations predict that seasonal groundwater hysteresis would dampen storm-scale stream network elasticity, thereby significantly increasing L-Q hysteresis on daily to monthly timescales ($p < 0.01$). Conceptual models of stream networks should consider the potential effects of groundwater hysteresis in headwaters catchments, especially in a changing environment. More broadly, our investigation highlights how spatially distributed process-based hydrological modeling can sometimes reveal emergent hydrological behaviors that are not apparent from sparse field data.

1 Introduction

Flowing stream networks interconnect global biogeochemical cycles across all timescales (Aufdenkampe et al. 2011, Castro and Thorne 2019, Allan et al. 2021, Liu et al. 2022). Headwater streams (i.e., streams without tributaries) account for the majority of network length (Downing et al. 2012) and fulfill a unique environmental role (Clarke et al. 2008, Wondzell 2011, Von Schiller et al. 2017) characterized by expansion, contraction, and disconnection in response to patterns of landscape

https://doi.org/10.5194/egusphere-2025-6294
Preprint. Discussion started: 12 January 2026

wetting and drying (Gregory and Walling 1968, Prancevic et al. 2025). Climate-mediated streamflow regime changes can have cascading effects on fluvial systems and stream ecology (Dhungel et al. 2016), including reducing the total extent and spatial connectivity of flowing stream networks in ways that are challenging to predict and manage (Jaeger et al. 2014, Ward et al. 2020, Botter et al. 2021). Changes to the extent and persistence of flowing stream networks can have large-scale consequences for freshwater ecosystems, carbon fluxes, nutrient cycles, and other fluvial processes (Alexander et al. 2007, Freeman et al. 2007, Meyer et al. 2007, Marx et al. 2017).

Flowing stream networks are coupled to local groundwater (GW) conditions (Freeze and Cherry 1979, Winter et al. 1999). Although intense precipitation can cause ephemeral streamflow over dry soil (Kampf et al. 2016), on longer timescales, flowing stream network variability is the surface expression of varying GW levels (De Vries 1995). As GW converges from hillslopes to valley bottoms, streamflow (Q) initiates where the total down-valley flow exceeds the subsurface conveyance capacity (Carlston 1963, Hewlett and Hibbert 1967, Godsey and Kirchner 2014, Ward et al. 2018), which is controlled by spatial patterns of upslope wetness, down-valley topography (valley bottom width and slope), and hydrogeological properties (transmissivity). Numerous studies have mapped flowing stream network variability by visual observation (e.g., Godsey and Kirchner 2014, Whiting and Godsey 2016, Jensen et al. 2017, Durighetto et al. 2020, Senatore et al. 2021), distributed sensors (e.g., Jensen et al. 2019, Zanetti et al. 2022), and remote sensing (e.g., Dugdale et al. 2022, Dralle et al. 2023).

Observational studies suggest a power law scaling relationship between Q and the length of the upstream flowing network (L), i.e., $L \sim Q^{\beta}$, with β varying from near zero to greater than 0.5 largely depending on topography (Prancevic and Kirchner 2019). The β exponent is also referred to as the "elasticity coefficient" since it describes the flowing network elasticity in response to changing catchment wetness (Prancevic et al. 2025). As GW levels rise, flowing streams also receive additional inflow due to changing hydraulic gradients (Zimmer and McGlynn 2017a), and thus Q increases proportionally faster than L ($\beta < 1$). The power law exponent (β) describes the relative scaling between fractional changes in Q and L under the assumption that Q and L are instantaneously coupled. In this study, we challenge the assumption of instantaneous hydrological coupling that is implicit in the power law approximation. Although proponents of the L-Q power law acknowledge that it is an approximation, the suitability of this approximation is based on a handful of labor-intensive stream network surveys, which do not constrain the full range of hydrological variability on daily to decadal timescales. For example, the hysteresis behavior analyzed in the present study only becomes apparent from many years of daily stream network length estimates, which cannot realistically be reproduced by intensive field surveys. From the current sparse field observations, it thus remains unclear whether a fixed monotonic L-Q scaling relationship is suitable for analysis in nonstationary environments. Conversely, process-based hydrological reasoning gives us a reason to doubt that the L-Q relationship would be monotonic in nonequilibrium conditions.

https://doi.org/10.5194/egusphere-2025-6294
Preprint. Discussion started: 12 January 2026

Groundwater responds to terrestrial water inputs more slowly than streamflow due to threshold-like soil saturation processes (Beven 2006, Spence 2010), producing hysteretic relationships (temporally lagged responses) between GW and Q (Gu et al. 2023, Sproles et al. 2015, Andermann et al. 2012). Observations of the water table after rainfall or snowmelt runoff events indicate that hillslope GW generally lags Q (McGlynn et al. 2004, Allen et al. 2010, Camporese et al. 2014). This hysteresis can also reverse direction in riparian areas with shallow antecedent water tables (Q lags riparian GW) before hillslopes reach saturation (Kendall et al. 1999, McGlynn and McDonnell 2003). Antecedent wetness similarly decouples GW flow directions from topography (Van Meerveld et al. 2015) and mediates GW-Q hysteresis across runoff events (Detty and McGuire 2010, Penna et al. 2011). Since GW levels predominantly control L, the GW-Q hysteresis suggests a potential L-Q hysteresis grounded in well-established process-based reasoning and GW observations.

The hysteretic relationship between GW and Q is not considered by the power law L-Q scaling approximation, which implicitly assumes that all stream channels respond instantly and proportionally to the overall wetness of the entire watershed (Equation 2 of Prancevic et al. 2019). Prancevic et al. (2025) note this limitation in their extrapolation of the L-Q power law to 14,765 watersheds, but they suggest that the decoupling of Q from headwaters wetness is only relevant at scales >10,000 km^2. To the contrary, observations indicate a hysteretic relationship between L and Q even in small watersheds, with a longer network (shallower GW) during recession at catchment scales as small as 3.3 ha (Zimmer and McGlynn 2017b) and 2.6 km^2 (Zanetti et al. 2022). Moreover, catchment-scale observations at scales of 0.67 km^2 (Senatore et al. 2021) and 1.5 km^2 (Shaw 2016) show that Q sometimes varies substantially at constant L. Streamflow travel times can even introduce a reverse L-Q hysteresis during storms, with the network expanding rapidly while outlet streamflow increases gradually (Roberts and Archibold 1978, Jensen et al. 2019). Hysteresis effects are not necessarily limited to storm-event timescales though, as partial decoupling of L and Q is observed even at seasonal timescales (Blyth and Rodda 1973, Jensen et al. 2019). For example, the measured value of β nearly doubles (0.287 to 0.502) between winter and summer in a 0.41 km^2 catchment (Gregory and Walling 1968, reanalyzed by Godsey and Kirchner 2014). Nonmonotonicity in the L-Q relationship is thus apparent across a range of catchment sizes and timescales, in contrast to a bijective (1:1) power law. However, a lack of long-term timeseries data describing the L-Q relationship precludes precise estimation of the temporal lag between L and Q, and how that lag might vary with different environmental conditions. It remains unclear whether L-Q hysteresis is significant on the timescales that matter for fluvial and riparian environmental processes.

Although our general understanding of L-Q scaling is the result of empirical curve-fitting to field data, “bottom-up” approaches based on our physical hypotheses of how the system works at small scales can also be a useful means to explore the implications of our conceptual understanding (Hrachowitz and Clark 2017). Physically based, spatially distributed hydrological simulations are useful to investigate potential deviations from the L-Q power law relationship because mechanistic simulations enable process attribution, emergent spatial reorganization, and perturbation of climate conditions. Previous mechanistic approaches to simulating L-Q dynamics have spanned a range of complexity, from “perceptual”

https://doi.org/10.5194/egusphere-2025-6294
Preprint. Discussion started: 12 January 2026

models limited to the hyporheic zone (Ward et al. 2018), to semi-distributed models with lumped down-valley flow implicitly partitioned between Q and GW (Mahoney et al. 2023), to grid-scale distributed GW-Q models based on linear reservoirs (Gao et al. 2021). However, all of these approaches assume static GW pressure gradients based on the surface topography, in contrast to the time-varying behavior of observed GW levels (Zimmer and McGlynn 2017a , Van Meerveld et al. 2015). Fully dynamic GW-Q models that solve the three-dimensional Richards equation can successfully reproduce observed GW-Q hysteresis for individual wells (Camporese et al. 2014), but so far this type of model has only been applied to investigate the L-Q scaling dynamics of idealized theoretical catchments (Zanetti et al. 2024). Here, we implement a new medium-complexity bidirectional surface-groundwater coupling scheme within an existing spatially distributed physically based hydrology model to predict how GW modulates the effect of short- and long-term climate variability on flowing stream networks. We contrast our simulation results with the L-Q power law scaling relationship since it is widely used as the basis for empirical conceptualizations. Our simulation platform is based on the Distributed Hydrology Soil Vegetation Model (DHSVM, Wigmosta et al. 1994, Wigmosta and Perkins 2001), which is notable for representing mountain forest ecohydrological processes with high physical fidelity (Beckers et al. 2009) and is widely applied to examine the climate sensitivity of mountain streams (Cristea et al. 2014, Lee et al. 2020, Ridgeway and Surfleet 2021, Hasan et al. 2023).

Mountain catchments are expected to undergo extreme changes in places where precipitation shifts substantially from snow to rain, altering soil moisture, vegetation phenology, and streamflow timing (Thackeray et al. 2019, Harpold and Molotch 2015, Klos et al. 2014). The compounding effects of this change on L-Q dynamics remains uncertain, limiting our ability to predict and manage the future trajectory of fluvial systems. In general, a shift from snow to rain caused by warming is expected to increase streamflow "flashiness," with brief but frequent rainfall-runoff events replacing more gradual seasonal snowmelt (Foster et al. 2016, Kampf and Lefsky 2016, Patterson et al. 2022). However, prior L-Q scaling analyses have not permitted emergent reorganization of streamflow generation mechanisms and flow routing in nonstationary conditions; instead, prior studies assume a fixed hierarchical network activation sequence (Botter et al. 2021) or a fixed power law relationship between spatially distributed wetness and outlet Q (Ward et al. 2020, Lapides et al. 2021). Thus, the potential for climate-mediated disruptions to historical patterns of hydrological connectivity remains unknown.

We test the updated model in the 27 km^2 Sagehen Creek Basin (SCB, California, USA). Prior research on SCB reveals an extensive GW system that interacts with the underlying volcanic bedrock on multi-decadal timescales (Rademacher et al. 2001, 2005; Blumhagen and Clark 2008; Manning et al. 2012), though streamflow responds rapidly to variations in shallow riparian aquifers (Kirchner et al. 2020). SCB has a long legacy of ecohydrological monitoring, including a 16-year record of daily specific electrical conductivity (EC) data at the streamflow gauge location. Stream water EC reflects the accumulation of dissolved ions from mineral weathering processes along upstream GW flowpaths, which makes EC a useful tracer of temporally variable GW contributions from different parts of the landscape (Stieglitz et al. 2003, Brown et al. 2007, Cano-

https://doi.org/10.5194/egusphere-2025-6294
Preprint. Discussion started: 12 January 2026

Paoli et al. 2019, Warix et al. 2023). By synthesizing EC observations and physical modeling, we address the following questions:

(1) To what degree might GW hysteresis modulate the relationship between L and Q in a mountain catchment, and over what time scales is this hysteresis effect significant?
(2) How could GW mediate the sensitivity of L and Q during a partial snow-rain climate transition, and are simpler topographic water routing assumptions valid under changing runoff generation mechanisms?

2 Materials and Methods

2.1 Model Development

We substantially overhaul the water routing algorithms of a well-established hydrological model to enable simulation of the GW-L-Q interactions considered in this study. The original version of DHSVM (Wigmosta et al. 1994) assumed a topographic approximation for subsurface routing following the transmissivity parameterization from Beven (1982), and a later update implemented an explicit stream channel routing scheme based on linear storage reservoirs and Manning's equation (Wigmosta and Perkins 2001). Key changes to the present version include (1) recalculating hydraulic gradients (and hence GW flow directions) based on the spatially distributed water table at each timestep, (2) permitting lateral subsurface flow in grid cells containing channels, (3) instantiating a bidirectional surface-groundwater coupling based on the dynamic hydraulic gradient between stream water depth and the local water table, (4) recalculating channel hydraulic routing parameters at each timestep, and (5) implementing evaporation routines for flowing and dry channels.

The algorithmic implementations of subsurface flow and channel routing remain substantively unchanged, and the relevant equations are described by Wigmosta et al. (1994) and Wigmosta and Perkins (2001). No additional parameters are required by the new version of the model; instead, we simply leverage the existing parameters describing vertical and lateral subsurface heterogeneity within and between grid cells. Figure S1 gives an overview of geometrical relationships used to define stream and GW connectivity, and Fig. S2 shows how these relationships compare to the original model.

2.1.1 Dynamic Flow Directions and Gradients

The original model assigned flow to one or more of four neighbors (rook case), which has been revised to eight neighbors (queen case). The fraction of flow from one grid cell to any of its eight neighbors is proportional to the slope between the water table elevation of each pair of cells, defined by subtracting the water table depth from the grid cell elevation. Flow directions are recalculated each timestep based on the updated water table map. On a given timestep, a particular cell may

https://doi.org/10.5194/egusphere-2025-6294
Preprint. Discussion started: 12 January 2026

contribute flow to any number of neighbors between zero and eight depending on which (if any) neighbors have lower water tables.

2.1.2 Hyporheic Flow

The original model assumed that the water table never falls below the bottom of the channel in grid cells intersected by the channel network, and cell-to-cell (down-valley) subsurface flow was explicitly precluded in cells containing channels. The updated version permits down-valley hyporheic flow following the same water table-based subsurface routing scheme applied to non-channel grid cells. Unlike dedicated hyporheic models, which explicitly parameterize near-channel subsurface parameters that differ from the surrounding subsurface material (Ward et al. 2018), we apply the same grid cell average parameters to the hyporheic zone in DHSVM, which improves model parsimony since hyporheic channel fill thickness and conductivity data are sparsely available. Our approach requires no additional parameters (beyond what was previously required to operated DHSVM) and subsumes hyporheic zone heterogeneity within the "effective" parameters of the calibrated model, fitting with the approach to other lumped subsurface parameters in typical distributed model calibration frameworks. However, this simpler approach may contribute to network length overestimation if the hydraulic conductivity of the alluvial channel fill is underestimated.

2.1.3 Surface-Groundwater Coupling

The original model did not permit losing streams, i.e., streamflow could only flow out through the network, and could not recharge into GW. This assumption is more appropriate for the humid climate of Vancouver Island, where the DHSVM channel routing scheme was developed (Wigmosta and Perkins 2001). In the updated version, channels gain or lose water to the subsurface depending on whether the water level in the channel (CWL) is above or below the grid cell water table. The CWL is calculated each time step based on the storage (related to Q through a linear reservoir equation) and the channel segment length, depth, and width (Fig. S1). If the CWL is below the local groundwater level (GWL), the channel gains water via lateral inflow from GW, and if the water table is below the CWL but above the channel bottom, the channel loses water via lateral outflow to GW. In both cases, the hydraulic gradient is calculated on each timestep based on the channel geometry and the difference in elevation between the CWL and the GWL. Transmissivity is determined by integrating the depth-variable conductivity in each grid cell over the vertical distance between the CWL and the GWL. If the water table is below the bottom of the geomorphic channel, Q recharges GW through vertical infiltration, determined by the vertical hydraulic conductivity and the gradient between the CWL and the GWL. To reduce the dependence of surface-groundwater coupling dynamics on the (arbitrary) grid scale resolution, the water table directly below the channel can vary separately from the grid cell average water table, with lateral conveyance away from the recharge zone calculated using the same approach to lateral hydraulic gradients and transmissivity introduced previously. This linkage permits the emergence of GW mounding and

https://doi.org/10.5194/egusphere-2025-6294
Preprint. Discussion started: 12 January 2026

hyporheic flow at the sub-grid-cell scale. Moreover, individual stream reaches may alternately gain or lose GW at different times, as sub-grid-scale hydraulic gradients are recalculated on each time step in response to the current GWL and CWL. The seasonal behavior of lateral inflow, lateral outflow, and vertical recharge from different stream orders is illustrated in Fig. S10.

2.1.4 Dynamic Stream Routing

The original model assumed static values for the hydraulic radius and slope required by Manning's equation, based on an arbitrary reference flow and the topographic slope, respectively. In the updated version, the hydraulic radius is recalculated each timestep based on the channel geometry and dynamic water depth, which accounts for the way that channels become relatively more rough as water increasingly interacts with the textured channel bed at low flows. Additionally, the stream surface slope, also used in Manning's equation, is now calculated on each timestep, which permits the model to develop transient backwater effects. The water depth at the lower end of each reach is assumed to match the water depth at the top of the downstream reach, and the water depth at the top of each reach is calculated from mass conservation assuming a uniform slope within each reach. The difference in water depth between the top and bottom of each reach thus determines a transient gradient that is added to the channel bed (topographic) slope in Manning's equation. Stream water depths and slopes are propagated uphill starting with a uniform depth at the outlet. The updated stream routing scheme enables emergent interactions between flow rates and downstream ponding in flatter reaches, which smooths streams over subtle knickpoints and permits a more realistic relationship between Q and GW levels throughout the flowing network.

2.1.5 Stream Channel Evaporation

The original model did not parameterize evaporation from stream networks. In the updated version, the existing Penman-Monteith implementation of potential evapotranspiration (PET) is applied to calculate evaporation from flowing stream channels, assuming that open water channel evaporation occurs at the potential rate, with surface area defined by the channel width and reach length. For channels that are dry, soil evaporation is implemented based on the extant soil desorption process in DHSVM. In grid cells with channels, understory fractional coverage is reduced in proportion to the channel surface area, but overstory fractional coverage is unchanged since riparian trees may overhang the channel. Although evaporation from flowing streams is usually a small fraction of the water balance (e.g., 0.4% of total ET in our SCB simulation), we find that it is nevertheless an important process that often determines the persistence or drying of very small streams (on the order of 0.001-0.1 liter/s).

https://doi.org/10.5194/egusphere-2025-6294
Preprint. Discussion started: 12 January 2026

2.1.6 Technical Considerations

Several nuances of the actual programmatic implementation are relevant for understanding our L-Q coupling simulations. DHSVM defines stream networks with reaches of arbitrary length, set at 30 m in this study, though most studies use much longer reaches defined only by the network topology (i.e., each tributary is a single reach). Importantly, the stream network topology is independent of the grid scale resolution (10 m in this study); one reach frequently spans multiple cells, and cells at confluences can have two or more reaches. Thus, the many-to-many relationship between streams and cells is nontrivial. These relationships are considered carefully in the implementation here, such that (1) water added to a stream from the subsurface is only available for recharge or evaporation in cells downhill of where it entered the channel, and (2) all incoming streamflow in a particular channel segment is fully available for recharge or evaporation in grid cells ordered sequentially downstream (i.e., a stream can recharge its entire flow into a single grid cell if that cell has sufficient dry pore space).

DHSVM equations are implemented using an "operator splitting" approach (Clark and Kavetski 2010), with all processes assumed constant over the (arbitrary) discrete time step, but real hydraulic gradients vary continuously through time. The updated version of the model only permits GW flow to the extent that would bring water tables into equilibrium within a single time step (i.e., water cannot continue flowing from cell A to cell B during a single time step if that would raise the water table of cell B above cell A). This reduces unphysical oscillations caused by the reversal of flow directions as minor water table variations propagate through low-relief areas. Additionally, for grid cells where the change in water table depth across a given time step is greater than the elevation separation from its down-gradient neighbors, hydraulic gradients are averaged between the current and previous time steps on the basis that the hydraulic gradient changes continuously over time, not instantaneously. An analogous approach is applied to the channel water level. This implies that the average flow rate within a single time step is equal to a linearized approximation of the continuously time-varying flow rate between the beginning and end of the time step. Note that the time-averaging of hydraulic gradients is only applied in areas with very low gradients at times in which the water table is changing rapidly; under other conditions, the instantaneous water table is assumed to be a reasonable approximation over whole time steps. This approach is congruent with a similar strategy applied to vertical unsaturated flow in the original version of DHSVM (Equation 42 of Wigmosta et al. 1994).

A video animation of simulated GW flow in SCB (Supplemental Material) shows remarkably complex patterns of GW activation that intuitively match expectations for the way that water would flow over complex topography. Repeated visualization and manual tracking of water through the model helped identify many of the complex nuances addressed above. We suggest that animated visualizations are underutilized to help elucidate whether complex models are (or are not) matching intuition for the way that water does (or does not) move. Additionally, this visualization provides insight into how

https://doi.org/10.5194/egusphere-2025-6294
Preprint. Discussion started: 12 January 2026

antecedent conditions create emergent streamflow generation patterns, but of course we do not expect the animation to match the actual spatial locations of GW flowpaths due to uncertain subsurface heterogeneity.

2.2 Model Application

We apply the updated version of DHSVM to simulate L-Q dynamics in SCB. The model is discretized at 10 m horizontal resolution, with stream segments of 30 m maximum length, and at a 3-hour time step. Initiation points of the geomorphic channel network are determined from the National Hydrography Database (NHD, U.S. Geological Survey 2019). Compared to the standard DHSVM setup approach, which initiates channels based on a minimum upslope contributing area, the NHD-based approach better represents the heterogeneity of channel density: for example, the western edge of the basin has a denser channel network compared to the northern edge (Fig. S3). Numerous studies indicate that map-based stream databases tend to underestimate stream network extent (e.g., Fritz et al. 2013, Lapides et al. 2021). However, in our specific SCB study watershed, the NHD-based network is much more extensive than the largest observed flowing network (compare Fig. 1 of Godsey and Kirchner 2014 with Fig. 1 of this study), though some of the channels and confluence locations are imprecise. For the sake of greater generality, we do not manually refine the SCB stream network, preferring instead to test the ability of existing datasets (i.e., NHD) to reproduce key aspects of stream network elasticity in DHSVM in order to build towards large-domain modeling. Reach-scale transmissivity variations are uncertain regardless, so we prefer to treat the simulated streams as representative counterparts of the actual network without expecting a 1:1 correspondence between individual modeled and measured stream reaches. The watershed modeling domain is extended approximately 2 km below the stream gauge (USGS site 10343500) to reduce the effect of unknown boundary conditions on the partitioning of down-valley flow between Q and GW at the calibration point (Fig. S3).

The rectangular geometry of each channel reach (depth and width) is estimated from regional power law regressions related to contributing area developed by Bieger et al. (2015). We refine the estimation of channel width by adjusting the parameters to more closely match stream widths measured at 17 locations across five representative reaches in Google Earth, which span a per-reach mean range of 0.8 to 3.4 m (contributing area 1 to 31 km^2). The refined equation relates channel width to contributing area with a power law scale of 0.85 and exponent of 0.41, which achieves R^2 = 0.98 across the five representative stream reaches. Channel depths predicted by the Bieger et al. (2015) data generally match with our expectations from field experience in SCB, e.g., 0.2-0.5 m bank cut height. We constrain the channel depth and width to minimums of 0.1 and 0.25 m, respectively, roughly congruent with field observations. Note that we do not consider small soil rills as part of the geomorphic channel network. Channel roughness (Manning's N coefficient) is estimated from a regression equation compiled by Limerinos (1970) and a d84 particle size of 0.25 m, roughly representative of headwaters mountain streams. Our prior manual sensitivity tests have indicated minimal sensitivity of DHSVM to channel roughness. Although the channel geometry is undoubtedly a source of uncertainty in our analysis, we emphasize that the dynamic water

https://doi.org/10.5194/egusphere-2025-6294
Preprint. Discussion started: 12 January 2026

table gradients are adaptable to over- or under-estimation of the channel geometrical proportions, since the water table will dynamically rise to the level necessary to interact appropriately with the stream, which is constrained by calibration at the outlet gauge, network field surveys, and geochemical timeseries.

Considerable spatial information (Fig. S3) and other parameters are required to operate DHSVM. Baseline parameters are estimated from prior literature reviews, as documented in Boardman et al. (2025). Land surface cover, vegetation type, and fractional cover are estimated from NLCD, LANDFIRE, and RCMAP, respectively (Dewitz and U.S. Geological Survey 2019, LANDFIRE 2022, Rigge et al. 2021). Subsurface heterogeneity is represented by disaggregating regional soil survey data from SSURGO (Soil Survey Staff 2022) and water retention data (Gupta et al. 2022) based on topographic metrics using Random Forest (Breiman et al. 2002). The relative pattern of bedrock depth is estimated by combining disaggregated SSURGO data with a curvature-based approach (Patton et al. 2018), and up to 20 m of sediment fill is added in low-gradient areas following the approach of Essaid and Hill (2014) in SCB. We emphasize that maps of subsurface properties are not expected to match actual spatial heterogeneity, but as in the case of the imperfect channel network, introducing a representative degree of spatial variability (inferred from regional databases) should help increase the physical realism of our simulations even if the spatial patterning is inexact. Daily gridMET meteorological data (Abatzoglou 2013) are disaggregated to the 3-hour model timestep using the MetSim preprocessing routine (Bennett et al. 2020).

Key model parameters with high uncertainty are refined via calibration in a multi-objective Bayesian optimization framework (Jones et al. 1998, Boardman et al. 2025). The calibration period is water years 2015-2024, and the validation period is 2001-2014 (overlapping the available EC measurements from 2001-2016). A five-year spin-up period is used to control for unknown initial conditions. A total of 14 parameters are calibrated simultaneously, including additive or multiplicative adjustment factors applied to bias-correct the gridded temperature and precipitation data, respectively (Boardman et al. 2025). The following parameters are determined by spatially variable maps calibrated relative to a mean value: soil depth, hydraulic conductivity, the exponential decrease in conductivity with depth, porosity, field capacity, overstory leaf area index, and overstory fractional cover. The following parameters are calibrated based on look-up tables: minimum stomatal resistance (variable across vegetation types, calibrated relative to mean), the maximum air temperature for snowfall, the accumulation- and melt-season snow albedo decay rates, and the threshold to increase albedo with new snow. Calibration is implemented using six objective functions: daily Nash-Sutcliffe Efficiency (NSE), daily log-scale NSE, mean absolute yearly percent error, mean absolute percent error between April and July (snowmelt season), root mean square error in > 95th-percentile high flows, and mean absolute yearly peak flow percent error. Due to parameter interactions that reduce the effective dimensionality of the parameter space and a highly efficient sampling algorithm that rapidly improves the Pareto frontier using surrogate model optimization procedures, we can calibrate DHSVM using many fewer optimization runs than might be expected given the dimensionality of the search space (cf. correlograms in the Supplement to Boardman et al. 2025). Additionally, we accelerate the calibration through pre-calibration at coarser resolutions of 30 and

https://doi.org/10.5194/egusphere-2025-6294
Preprint. Discussion started: 12 January 2026

90 m (Sun et al. 2020). Among 760 total tested models (360 tested at 10 m resolution), we select 30 calibrated models with diverse parameter values that all achieve < 20% mean absolute error for the annual water yield. Although all six objective functions are used during calibration, we include several models with sub-optimal streamflow goodness-of-fit in this 30-member ensemble in order to evaluate the sensitivity of L-Q scaling dynamics to the model parameters (Fig. S5 and Fig. S6).

We simulate daily L-Q scaling dynamics for 30 parameter subsets and compare the simulated power law anomaly (L_A) with measured anomalies in electrical conductivity (EC_A). Only a few parameter sets achieve both satisfactory NSE and reasonably high seasonal L_A-EC_A correlation, indicating skill at simulating both surface streamflow variability and GW flowpath variability. We select the model with the highest seasonal L_A-EC_A correlation since the L_A anomaly is our primary focus in this study. The selected parameter set has several other desirable characteristics compared to other tested parameters, including reasonably high NSE and log-scale NSE on both calibration and validation periods (calibration: 0.78, 0.82 log, validation: 0.61, 0.76 log, overall: 0.71, 0.79 log). Additionally, the selected parameter set has a relatively small median network size that is closer to field-surveyed L compared to other tested parameter sets (Fig. S6).

The relationship between parameter uncertainty and L-Q scaling is illustrated in Figs. S5-S6. In general, higher transmissivity is associated with smaller, more dynamic networks. Most of the acceptable parameter sets (total NSE and log NSE > 0.7) produce L-Q power law exponents (β) within the range of uncertainty from field surveys (Godsey and Kirchner 2014). Only three tested parameter sets have acceptable NSE and an L_A-EC_A correlation stronger than -0.8. Of these, the selected parameter set is closest to the field-measured β with the smallest median length (closest to field surveys). Thus, we use this parameter set for our primary L-Q simulations.

We evaluate L-Q dynamics by saving maps of Q for each of 2,382 unique stream reaches within SCB at noon on every day between October 1, 2000, and September 30, 2024 (8,766 days). This results in a total of $2x10^7$ datapoints (number of reaches times number of days) describing the spatiotemporal evolution of the flowing stream network. In contrast to the four datapoints available in the same catchment from field surveys, we hypothesize that the massive scale of data generated by process-based models may provide different insights from rare field surveys.

2.3 Statistical Analysis

All significance values are calculated using the one sample two-sided t-test, or the Pearson's product-moment correlation test, implemented in the R statistical programming language.

We define the outlet streamflow, Q, as the daily modeled flow rate in units of specific discharge (area normalized). We define the flowing network length, L, as the sum of lengths of all upstream reaches with non-zero simulated outflow. We

https://doi.org/10.5194/egusphere-2025-6294
Preprint. Discussion started: 12 January 2026

also test an alternate definition of L using a minimum flow threshold of 0.01 liter/s to define "flowing" reaches. This alternate definition provides a nearly identical timeseries of L (r = 0.9997). For simplicity, we adopt the simple non-zero streamflow definition (arbitrarily low streamflow still counts as "flowing") for the remainder of this study.

The crux of our study is a comparison between DHSVM-simulated L and a power law function, $L_P(Q)$, defined as follows:

$$L_P = \alpha Q^{\beta} \quad (1)$$

We estimate α and β through least-squares regression of L and Q in log-log space, where Equation 1 is linear. We only consider L-Q pairs with Q < 2 mm/d to control for the asymptotic behavior of L at high Q, as L approaches the maximum geomorphic network extent (subsequently illustrated in Fig. 3). In our study, the best-fit values are α = 45.54, β = 0.2705.

The residual between L (simulated by DHSVM) and L_P (power law prediction from the same DHSVM-simulated Q) defines the network anomaly, L_A:

$$L_A = L - L_P \quad (2)$$

We calculate the autocorrelation of L and L_P to evaluate the degree of hysteresis that is not explained by a bijective (1:1) relationship between L and Q (Fig. S11). The sample autocorrelation $R_L(k)$ of the discrete L(t) timeseries at a lag k (in days) is estimated as follows (Venables and Ripley 2002), where n is the number of samples in L, σ^2 is the sample variance, and μ is the sample mean:

$$R_L(k) = \frac{1}{(n-1)\sigma^2}\sum_{t=1}^{n-k}(L(t)-\mu)(L(t+k)-\mu) \quad (3)$$

The "hysteresis effect" is defined as the difference in DHSVM-simulated autocorrelation relative to the power law autocorrelation (R_{LP}), defined analogously to R_L by replacing L(t) with $L_P(t)$. The network length hysteresis effect, HE_L, is thus:

$$HE_L(k) = R_L(k) - R_{LP}(k) \quad (4)$$

Defining the hysteresis effect this way provides a metric with an easily interpretable range of values (same scale as [0,1] range of autocorrelation) that can directly quantify hysteresis at various discrete time lags.

We calculate R_L, R_{LP}, and HE_L at lags of k = 0 to 180 for the entire 24-year timeseries as well as separately within 24 "block bootstrap" subsets defined by each water year (October 1 through September 30), extended backwards and forwards 90 days to reduce the impact of the arbitrary start date for longer values of k. Thus, each of the 24 block bootstrap samples overlap a total of 180 days, with the exception of the first and last water years, which only overlap 90 days in one direction. We use these 24 estimates of HE_L to evaluate the statistical significance of HE_L at different lags using a one sample two-sided t-test.

Analogously to Equations 1-4, we use measured EC data to calculate a best-fit power law (EC_P), anomaly (EC_A), autocorrelation (R_{EC}), power law autocorrelation (R_{ECP}), and hysteresis effect (HE_{EC}). For EC, we only consider block bootstrap periods with no more than 25% missing data, which yields 15 usable bootstrap periods.

https://doi.org/10.5194/egusphere-2025-6294
Preprint. Discussion started: 12 January 2026

To relate variations in HE_L and HE_{EC} to variations in snow and rain partitioning, we aggregate DHSVM-simulated watershed-average snowfall and precipitation within each of the same block bootstrap periods. The snow fraction is defined as the fraction of watershed-average precipitation falling as snow. Finally, we apply the Pearson's product-moment correlation test to estimate the correlation between the snow fraction and either HE_L or HE_{EC} at lags of 10, 20, and 30 days.

3 Results

3.1 Flowing Stream Network Dynamics

Simulated flowing stream networks expand, contract, and disconnect in response to variable wetness in SCB (Fig. 1). The model reproduces observed daily, seasonal, and interannual variations in Q across the 24-year simulation period, with a Nash-Sutcliffe Efficiency (NSE, equivalent to R^2) of 0.79 for log-transformed daily Q. Importantly, the model also reproduces the network elasticity observed by field surveys (Godsey and Kirchner 2014), with a model estimate of $\beta = 0.27$ and a field estimate of $\beta = 0.31 \pm 0.09$. There is considerable uncertainty in field-based validation of the absolute network length due to model variability in L at constant Q, but the model likely overestimates L due to a combination of network digitization artifacts and uncertain transmissivity in the hyporheic zone (i.e., channel fill). To maintain simplicity in our definition of a "flowing stream," we calculate L wherever Q is nonzero (cf. sensitivity test in Section 2.3), which makes L sensitive to small Q that might not be detected in the field (Sarah Godsey, personal communication, October 2025). The survey dates from Godsey and Kirchner (2014) are only reported to the nearest month, and personal communication with the first author of that study (Sarah Godsey, December 2024) indicates that the channel network survey data have likely not been preserved outside of the figures from that study, rendering an exact comparison impossible. Furthermore, the absolute stream network length is ill-defined because stream networks have a fractal dimension greater than one (Mandelbrot 1982, La Barbera and Rosso 1989), so network length depends on the resolution of measurement. In our study, the 3 m DHSVM grid cells may provide a smaller "measuring stick" than the (unspecified) resolution used to measure channels by Godsey and Kirchner (2014), perhaps contributing to the discrepancy in absolute channel length. Regardless, for our sensitivity analysis of stream network elasticity, the absolute magnitude of L (power law scale) is less important than β (power law exponent), which matches field observations. Indeed, Godsey and Kirchner (2014) only report the best-fit power law exponent and do not to report the best-fit power law scale, supporting our contention that the power law scale is relatively unimportant for overall hydrological understanding. Our model simulations predict frequent stream disconnection, i.e., dry channel gaps that interrupt the flowing network (Fig. 1), which is also in qualitative agreement with the mapped network behavior (Godsey and Kirchner 2014), although exact disconnection locations are imprecise due to uncertain fine-scale heterogeneity.

https://doi.org/10.5194/egusphere-2025-6294
Preprint. Discussion started: 12 January 2026

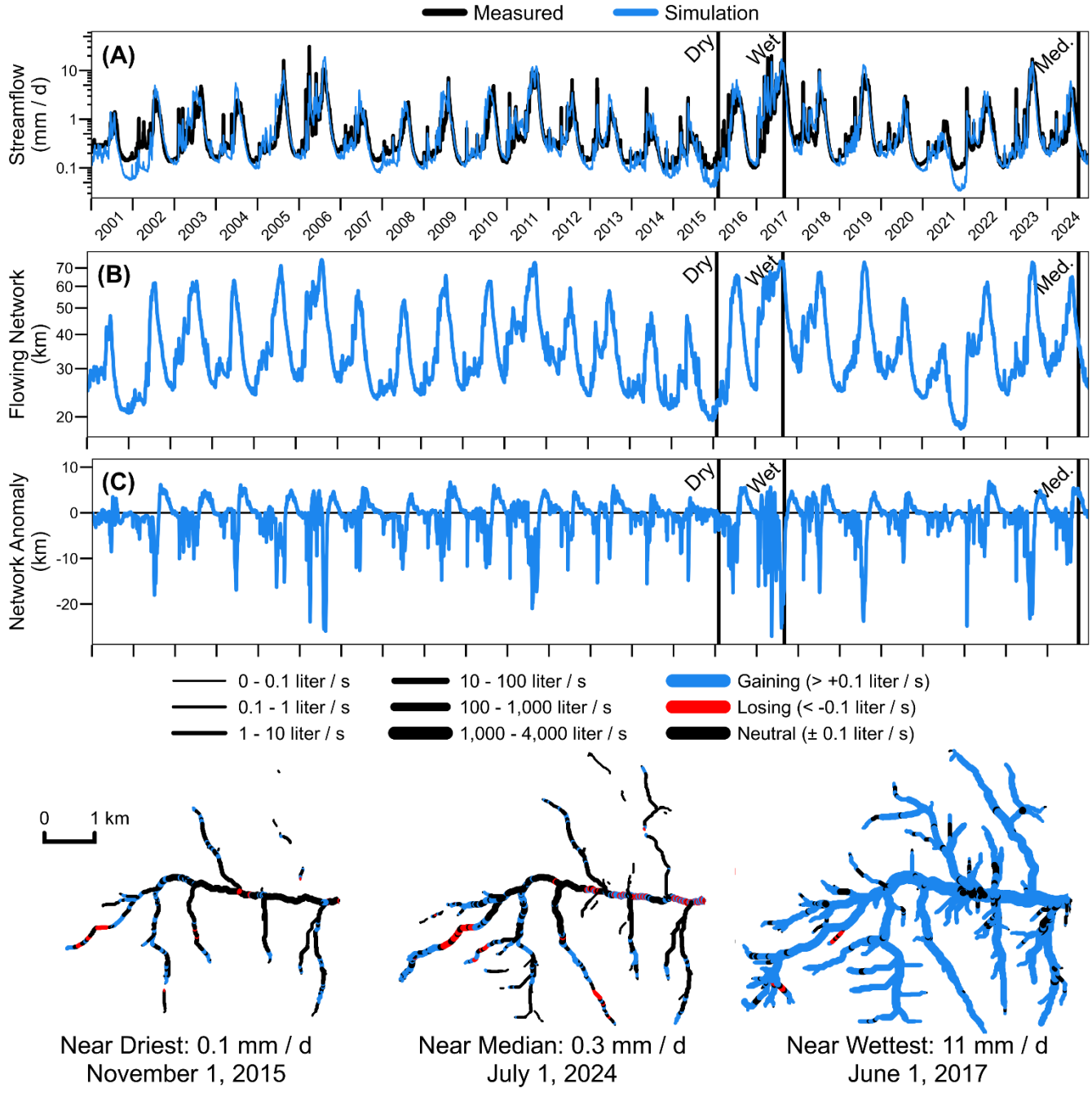

Figure 1. Daily timeseries over the 24-year study period: (A) measured and modeled streamflow, Q, (B) modeled flowing stream network length, L, and (C) modeled anomaly in L relative to a power law scaling assumption. Example maps of the modeled flowing network show the spatial arrangement and variable Q (line width) of flowing stream reaches at 1st, 50th, and 99th-percentile flows. Stream reaches that are gaining Q from GW are illustrated in blue, reaches that are recharging Q back to GW (losing) are illustrated in red, and reaches with an approximately neutral balance of inflows and outflows are illustrated in black.

https://doi.org/10.5194/egusphere-2025-6294
Preprint. Discussion started: 12 January 2026

In our simulations, higher-order stream reaches (downstream of confluences) are more stable over time, but the relationship between topography and L-Q scaling is nuanced. Streamflow persistence, defined as the fraction of time that a given reach is flowing, generally increases at larger Strahler order (Strahler 1957), as seen in Fig. S7 and similarly reported by Mahoney et al. (2023). Nevertheless, some first-order streams are perennial (persistence = 100%), and some third-order streams have persistence as low as 36% (Fig. S7). (In this context, we consider a static Strahler order based on the geomorphic channel network, not the flowing network.) Further, there is only a loose relationship between simulated stream persistence and the topographic wetness index (Fig. S8), challenging prevailing contributing area assumptions (Prancevic et al. 2019, Ward et al. 2018, Mahoney et al. 2023). In an alternate configuration of DHSVM with static hydraulic gradients defined by the surface topography (kinematic assumption as opposed to fully dynamic grid cell water table gradients), streamflow persistence is overestimated by a mean of 11% ($p < 0.01$) and watershed-average warm-season (July-October) evapotranspiration (ET) is underestimated ($p < 0.01$) by a mean of 8% overall and up to 25% on some days (Fig. S9). Topography-based routing schemes fail to account for the dispersion of GW recharge from streams into adjacent riparian corridors and broad valley bottoms, which subsidizes root-zone soil water (Tague and Peng 2013, Graup et al. 2022). Prevailing models used for prior L-Q analyses assume static topographic hydraulic gradients and flow directions (Gao et al. 2021, Mahoney et al. 2023), but our sensitivity analysis indicates that time-varying gradients and flow directions are more appropriate for L-Q analysis in the groundwater-driven SCB study watershed.

Lateral redistribution and convergence of GW into higher-order valley bottoms on seasonal timescales partially decouples the fractional contribution of different Strahler orders from the magnitude of outlet Q in our simulations (Fig. 2 and Fig. S10). Longer subsurface flowpaths in third-order valleys contribute a larger fraction of network-total lateral inflow (24-55%) in the late recession season (August-September) compared to the April-May snowmelt season (12-37%), when the shorter and faster hillslope flowpaths connected to first-order streams are more dominant. In our DHSVM simulations, GW recharge rarely exceeds 1% from fourth-order stream reaches (in contrast to smaller tributaries, where recharge is substantial), indicating that most higher-order valley bottom segments are consistently gaining water from the riparian aquifer (Fig. 2). This model prediction (which was not considered during model selection) is supported by observations of riparian water table levels from wells in the fourth-order SCB valley bottom (Kirchner et al. 2020), which likewise indicate that two particular locations along the fourth-order section of Sagehen Creek are consistently gaining water. In our simulations, most GW recharge is concentrated at the second and third Strahler orders of the geomorphic network, and there is only negligible recharge from the fourth-order reaches where the Kirchner et al. (2020) wells are located (Figs. 2 and S7).

https://doi.org/10.5194/egusphere-2025-6294
Preprint. Discussion started: 12 January 2026

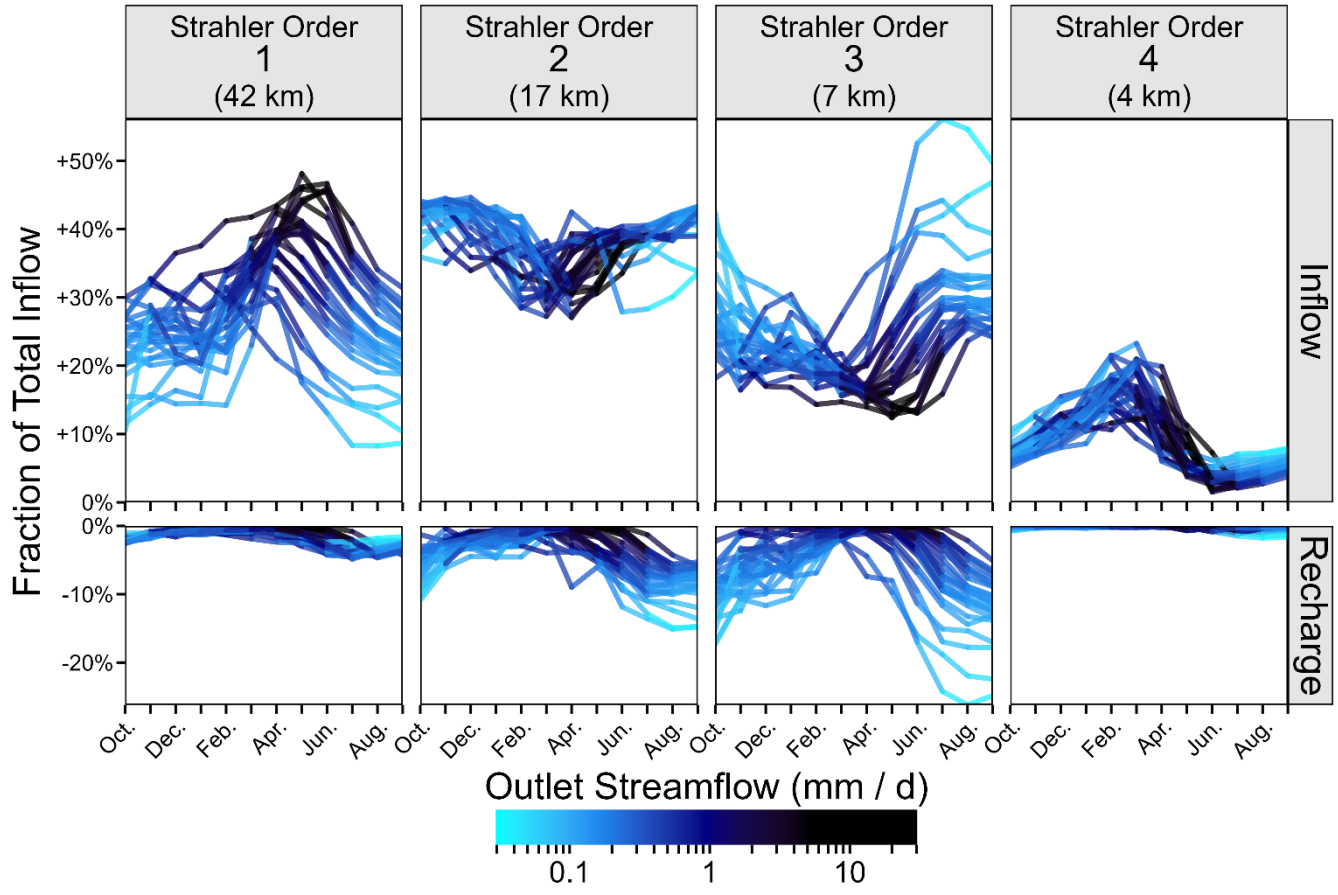

Figure 2. Seasonal variation in the inflow and groundwater recharge from stream reaches organized according to Strahler order (Fig. S7). Each line represents a single water year, and all values are aggregated to the monthly median. Lines are colored according to the log-scaled outlet streamflow, and the vertical axes are scaled in proportion to the total network inflow. First-order streams contribute relatively more inflow during the snowmelt period, and third-order streams contribute disproportionately in the late summer. Most recharge from streams to groundwater occurs in second- and third-order streams. Relative seasonal network dynamics are partially decoupled from the absolute magnitude of outlet streamflow.

3.2 Flowing Network Length Anomalies

Simulated L-Q scaling dynamics broadly reproduce the postulated power law relationship, albeit with substantial scatter (Fig. 3). We determine the best-fit power law function, $L_P(Q)$, using only days with simulated Q < 2 mm/d, because the notion of "flowing stream network" becomes ambiguous when surface flow exceeds the geomorphic channel network at high Q. This approach is consistent with other modeling studies that have used an upper threshold on Q to define the relevant power law scaling range for channelized flow (Gao et al. 2021, Mahoney et al. 2023), and field surveys in SCB suggest that the power law holds at least as high as 1.76 mm/d (Godsey and Kirchner 2014). The fitted power law has $R^2 = 0.91$ (below 2 mm/d), similar to the range of high R^2 values reported in field studies, e.g., 0.82-0.99 (Jensen et al. 2017). Nevertheless, this

https://doi.org/10.5194/egusphere-2025-6294
Preprint. Discussion started: 12 January 2026

high R^2 hides a systematic structure in the power law residuals, $L - L_P$, hereafter called the "network anomaly" or L_A (Fig. 1C).

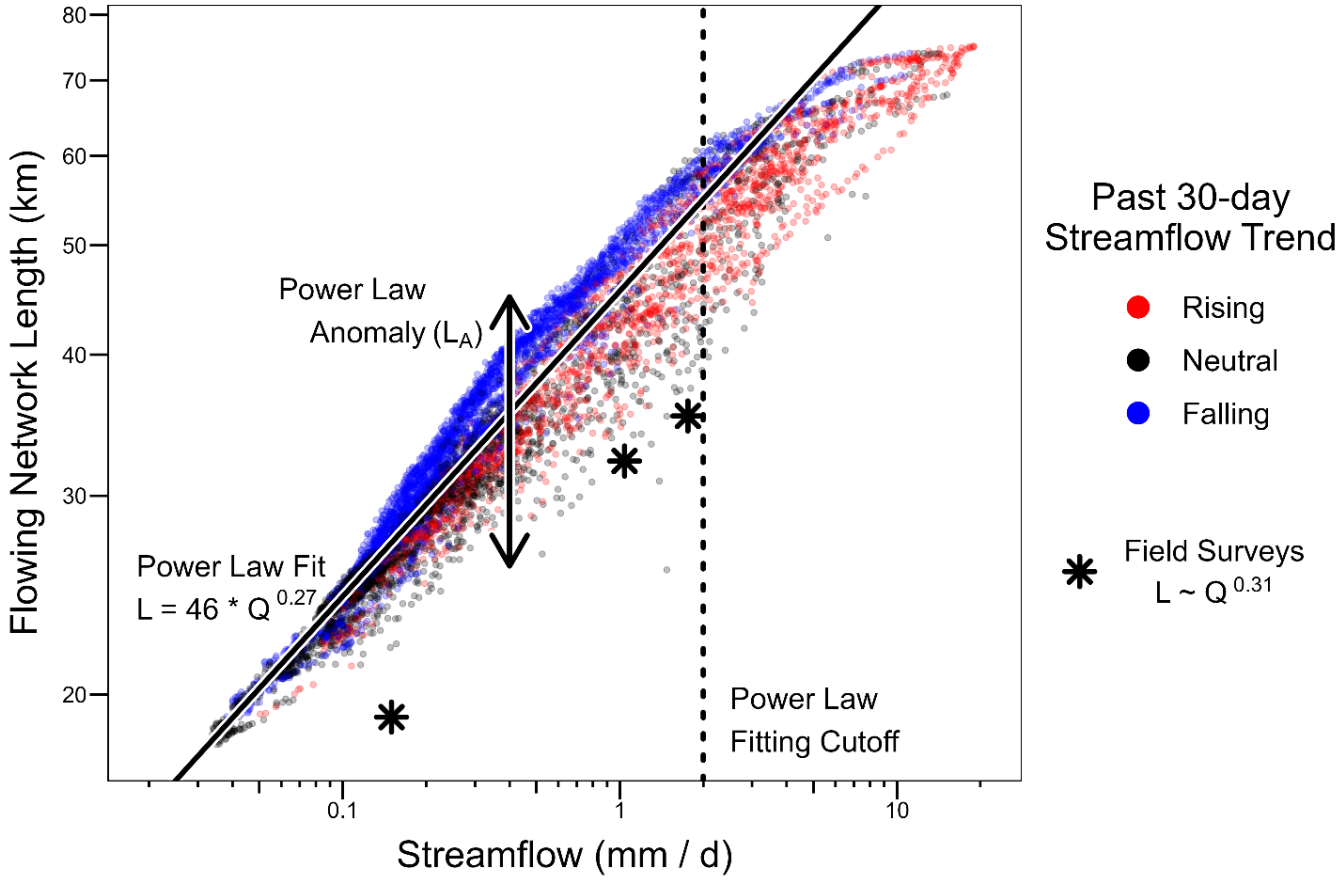

Figure 3. Logarithmically scaled scatterplot between simulated daily streamflow (Q) and flowing stream network length (L). Each point represents one day over water years 2001-2024. Red (blue) colors indicate a rising (falling) streamflow trend over the 30 days prior to each point. Three field surveys are shown, and a fourth survey falls below the lower vertical axis limit (Q = 0.24 mm/d, L = 15.4 km), which Godsey and Kirchner (2014) identify as a potential outlier because of practical difficulties in following the entire network on the first field survey.

Anomalously large stream networks for a given Q (positive L_A) are associated with a decreasing antecedent streamflow trend (recession period), whereas anomalously small networks for a given Q (negative L_A) are associated with an increasing or neutral antecedent streamflow trend. To explore this anomaly (on days with Q < 2 mm/d), we consider the sign of the Sen's slope of Q over the prior 30 days (Sen 1968) to determine the antecedent streamflow trend. Days with antecedent streamflow trends less than 1% per day relative to the current day's Q are considered neutral. As seen in Fig. 3, days with a rising streamflow trend have anomalously small flowing networks (mean L_A = -5.8%, $p < 0.01$), and the opposite is true during a

https://doi.org/10.5194/egusphere-2025-6294
Preprint. Discussion started: 12 January 2026

falling streamflow trend (mean L_A = +4.6%, $p < 0.01$). Neutral streamflow trends are associated with anomalously small networks (mean L_A = -3.5%, $p < 0.01$) because recession periods are relatively prolonged compared to periods of rising Q, which biases the power law to underestimate L during neutral flow periods in the least-squares fit.

By comparing the simulated network on specific days, we illustrate how (1) similar networks could produce widely varying Q, and (2) different network configurations with variable L could produce similar Q (Fig. 4). In the early recession season after seasonal snowmelt (June of 2013 and 2018), the simulated flowing network is anomalously large relative to the power law prediction, i.e., $L_A > 0$. In the late recession season (December), when antecedent conditions are relatively dry, rainfall-runoff events can elevate streamflow with only small increases in the flowing network. The 150% increase in Q between June 11, 2013, and December 18, 2023, would be associated with a 28% increase in L based on the best-fit L-Q power law, but our simulation shows a decrease of 0.4% instead since the two dates have different spatial water table configurations. In another example, an extra 10 km (+33%) of streams are flowing on June 12, 2018, compared to December 18, 2023, despite near-identical outlet Q on both days. Streamflow originating from high-elevation snowmelt in a relatively small headwaters reach may propagate down channels that would otherwise be dry, losing Q back to GW over lengths in excess of 0.5 km (Fig. 4) before reaching a downstream confluence. Thus, wetting of outlying headwaters reaches can have a disproportionate impact on the overall network extent without affecting outlet streamflow.

However, seasonal L-Q scaling anomalies are important for larger streams as well, not just trickling headwaters reaches. Considering the additional flowing stream reaches on June 12, 2018, that are dry during the storm event on December 18, 2023, these “extra” streams span a wide range of flow magnitudes, from near zero (< 0.01 liter/s) to as much as 39 liter/s (22% of outlet Q on both dates). This large relative contribution from different streams at different times indicates that the same downstream Q can derive from substantially different parts of the landscape depending on antecedent wetness and the resulting transient spatial GW configuration. In other words, the power law anomaly also manifests in sizable streams, not just trickling headwaters reaches.

https://doi.org/10.5194/egusphere-2025-6294
Preprint. Discussion started: 12 January 2026

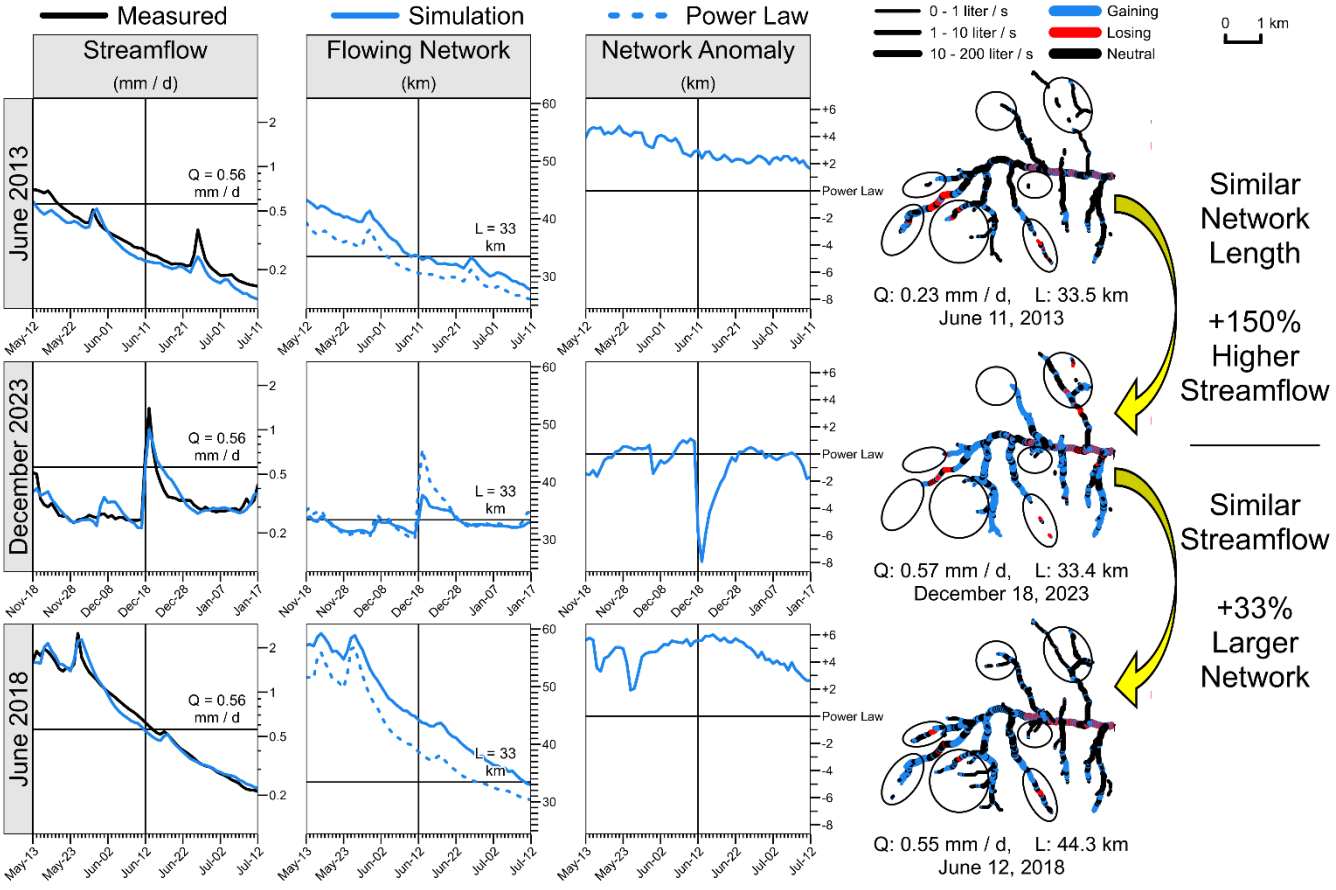

Figure 4. Examples of different streamflow magnitudes associated with the same flowing network size (June 2013 – December 2023) and different network sizes associated with equivalent streamflow (December 2023 – June 2018). Circled regions highlight parts of the flowing network that are particularly variable across these examples.

https://doi.org/10.5194/egusphere-2025-6294
Preprint. Discussion started: 12 January 2026

3.3 Chemical Signature of Groundwater Hysteresis

Measured daily EC at the SCB stream gauge generally correlates inversely with Q (more dilute concentrations of total dissolved ions at higher discharge), interpreted as an increased contribution from newer water (shorter subsurface residence time) during high flows. A power law fit between measured EC and Q gives a similarly high R^2 of 0.94 (Fig. S4), and the power law residuals (EC_A) exhibit a similar pattern to L_A. Days with a rising Q trend have anomalously high EC (mean EC_A = +1.8%, $p < 0.01$), and days with a falling Q trend have anomalously low EC (mean EC_A = -3.3%, $p < 0.01$). Anomalously high EC indicates an outsized contribution from longer subsurface flowpaths (older, more chemically evolved GW) during the rising hydrograph limb, consistent with the model prediction of anomalously small L under similar conditions.

Measured EC and simulated GW both show seasonal hysteresis loops with Q, which largely matches the seasonal pattern of L_A (Fig. 5). The modeled area-average catchment water table depth (WTD) is relatively deep (less GW storage) on the rising limb of the seasonal hydrograph (increasing Q), and relatively shallow (more GW storage) on the falling limb of the hydrograph (decreasing Q). Similar smaller loops are superimposed from individual rainfall or snowmelt runoff events. Again, measured EC shows a similar hysteretic relationship with Q, supporting the model results.

https://doi.org/10.5194/egusphere-2025-6294
Preprint. Discussion started: 12 January 2026

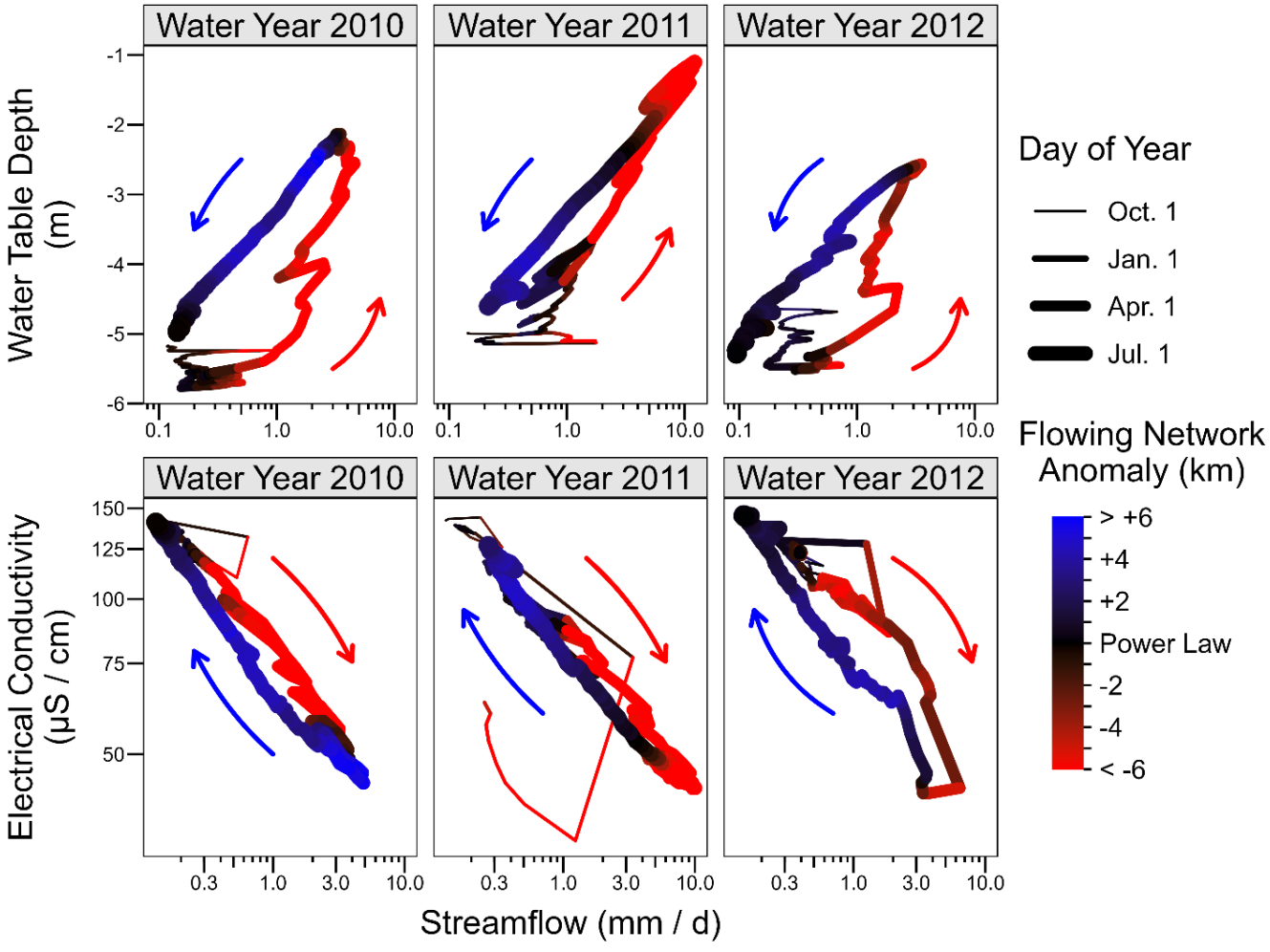

Figure 5. Hysteresis relationships in three example years, showing (top panels) simulated water table depth and simulated streamflow, (bottom panels) measured stream electrical conductivity, reflecting total dissolved ion content (correlated to groundwater age, Rademacher et al. 2001), and measured streamflow. Each line traces a path beginning on October 1st of a given water year, and line width is scaled proportionally to the day of year. Color indicates whether the simulated flowing stream network is larger (blue) or smaller (red) than predicted by a power law relationship with streamflow on a given day.

Measured EC_A mirrors simulated L_A, especially after aggregating the data over longer time periods to reduce the effect of uncertain model forcing and other sources of noise (Fig. 6). Across the 2001-2016 period of continuous EC monitoring, there are 4,750 days with available EC data and $Q < 2$ mm/d. Across this daily dataset, lower measured EC is strongly correlated with longer modeled L ($r = -0.87$, $p < 0.01$), but this correlation primarily reflects the mutual relationship with Q. After decorrelating L and EC from Q by subtracting the best-fit power law, EC_A and L_A are still significantly correlated, albeit more weakly ($r = -0.38$, $p < 0.01$). On daily timescales, other geochemical processes, random noise, and errors in the DHSVM forcing data would be expected to dilute the underlying GW hysteresis effect, potentially explaining this relatively

https://doi.org/10.5194/egusphere-2025-6294
Preprint. Discussion started: 12 January 2026

weak daily correlation. Aggregating both EC_A and L_A to the monthly median using only days with available EC data (176 months with at least two days of data) produces a stronger correlation of $r = -0.47$ ($p < 0.01$). Still, each year may have unknown and variable meteorological forcing biases that propagate into simulated GW, Q, and L, diluting the EC-L correlation. To further control for noise in the EC-L correlation, we also consider the overall seasonality of power law scaling anomalies in both EC and L by calculating the median for each month across all available years (Fig. 6). In this case, the seasonal pattern of EC closely mirrors L ($r = -0.95$, $p < 0.01$) and EC_A closely mirrors L_A ($r = -0.92$, $p < 0.01$). However, it is important to note that the monthly median L_A-EC_A correlation is considered as part of our model selection procedure (Section 2.2 and Fig. S5), so it is not independent evidence of the model's predictive skill. Nevertheless, the strong match between modeled network dynamics and measured stream chemistry supports our process-based GW hysteresis interpretation, and selecting the model that best matches observations (Fig. S5) increases the realism of our analysis.

https://doi.org/10.5194/egusphere-2025-6294
Preprint. Discussion started: 12 January 2026

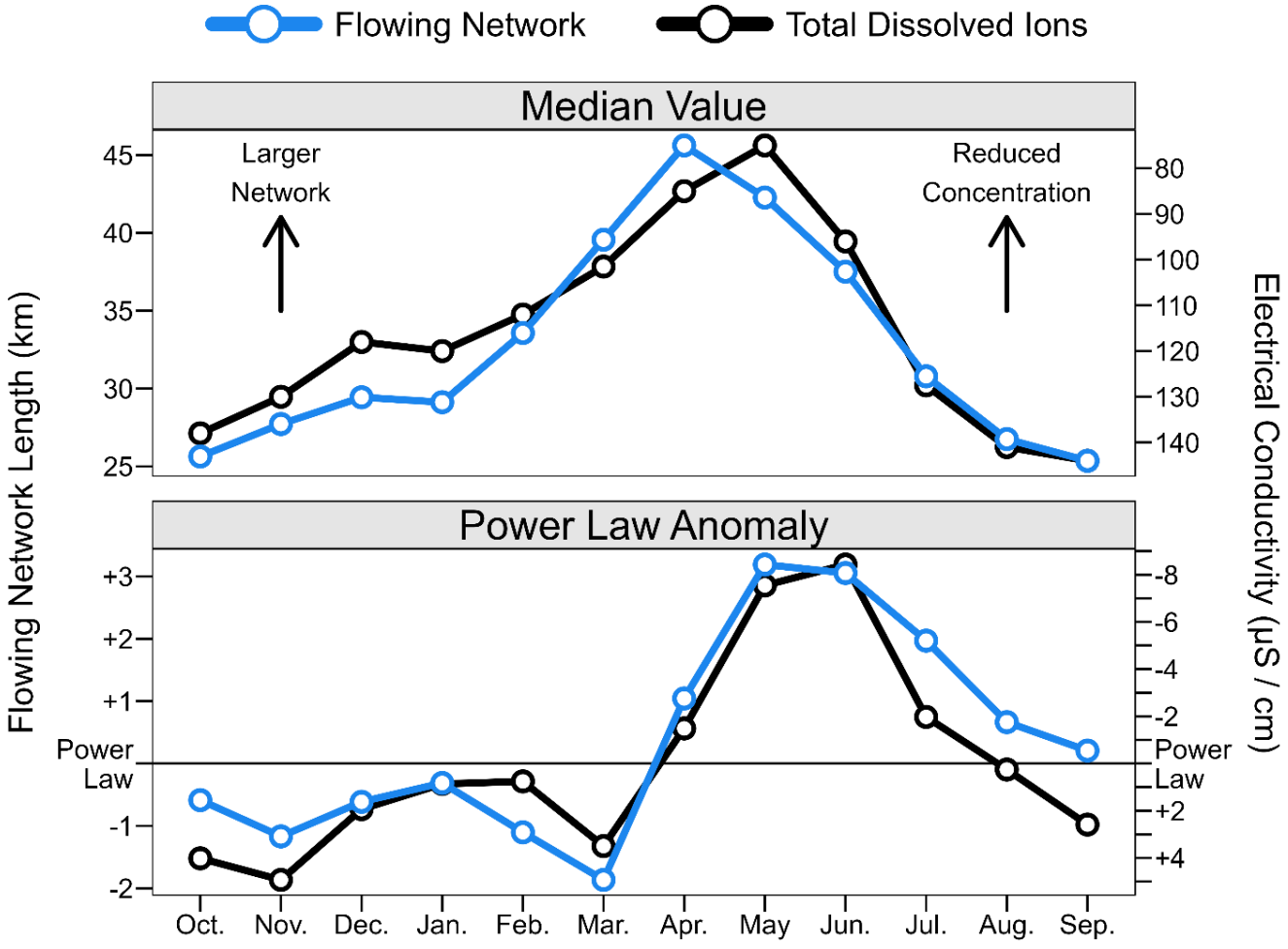

Figure 6. Comparison of monthly median simulated stream network dynamics with measured stream water electrical conductivity (EC), a proxy for total dissolved ion concentrations. Note that the vertical axis is reversed for EC (positive down) to highlight the similar shape of the seasonal signals. The seasonality of anomalously large flowing networks matches the seasonality of anomalously low EC, indicative of a greater fractional contribution from relatively fast, chemically dilute subsurface flowpaths during the snowmelt season.

3.4 Sensitivity to Snow-Rain Transition

In a warming climate, a partial snow-rain transition alters the spatiotemporal organization of liquid water inputs to the catchment, and simulating the cascading hydrological effects of this change (without untested assumptions of stationarity) requires a spatially distributed physical model such as DHSVM. We compare simulations of flowing stream network dynamics in the historical climate (Abatzoglou 2013) with a uniform +4 °C warming scenario applied to the same baseline climatology (2001-2024) to investigate the potential effects of a partial precipitation phase change. The +4 °C increase is

https://doi.org/10.5194/egusphere-2025-6294
Preprint. Discussion started: 12 January 2026

within the plausible range of cold-season anthropogenic warming in the SCB region (Null et al. 2010, Huang et al. 2018, Sun et al. 2019), but does not account for potential changes in other aspects of climate (e.g., precipitation timing and magnitude) or nuanced spatiotemporal controls on climate trends (Lundquist and Cayan 2007). Thus, the warming scenario implemented here should not be understood as a prediction of actual future climate sensitivity. Instead, we are concerned with the broad sensitivity of L-Q scaling assumptions to a transition from snow to rain, which is sufficiently captured by an easily interpretable uniform warming experiment. Over the 2001-2024 simulation period in SCB, a +4 °C warming scenario reduces the total fraction of precipitation falling as snow ("snowfall fraction") from 49% to 26%, i.e., total snowfall is reduced by 47% with the same total precipitation. Total streamflow is reduced by 8%, and annual peak flows change by -25% to +116% (median +5%), consistent with general expectations for reduced water yield and increased flood risk as mountains transition away from snow dominance (Berghuijs et al. 2014, Huang et al. 2018, Gordon et al. 2022).

Figure 7 illustrates salient characteristics of the snow-rain transition scenario using a single representative water year (2022). In this particular year of the +4 °C warming scenario, the predicted annual peak flow is 93 days earlier, 77% higher, and associated with a discrete storm event in December rather than a gradual snowmelt period in March and April. The annual median and minimum flows decrease by 28% and 35%, respectively. Based on the model simulation, the minimum, median, and maximum flowing network length each decrease by 13%, 10%, and 2%, respectively (in this example year), comparable to the 9%, 9%, and 3% reductions predicted for 1st-percentile, median, and 99th-percentile flowing network lengths across the full 24-year period. In contrast to the 2% decrease in maximum L predicted by the warming simulation in this year, the pre-warming L-Q power law predicts a 22% increase in maximum L, synchronous with the higher maximum Q. Naïve application of the power law assumption to simulated streamflow timeseries in a warming climate could thus misrepresent the directionality of changes in the maximum network extent. Even more dramatically, the power law predicts a maximum L during an October storm that is 77% larger than predicted by the simulation model (L = 37 km, L_P = 66 km). The power law L_P still overestimates the DHSVM-simulated maximum L during this late-recession-season storm by 45% in the historical climate, but the near-complete transition to rain for this storm (2% vs. 35% snow fraction) increases the importance of considering the spatial configuration of antecedent GW levels. In the 2022 example year (Fig. 7), and throughout the longer simulation period, the power law systematically underestimates DHSVM-simulated L during seasonal recession periods (panels B-C). In the warmer climate, the power law underestimates DHSVM-simulated L ($p < 0.01$) by a median of 7% (interquartile range: 5% to 11% underestimation) over the 137-day period from maximum L (January 15) through the end of May. This underestimation is even more apparent during the snowmelt recession period in the historical climate, when snow is more dominant: over the 98-day period from maximum L (April 25) through the end of July, the median underestimation relative to DHSVM is 11% ($p < 0.01$, interquartile range: 9% to 13% underestimation).

https://doi.org/10.5194/egusphere-2025-6294
Preprint. Discussion started: 12 January 2026

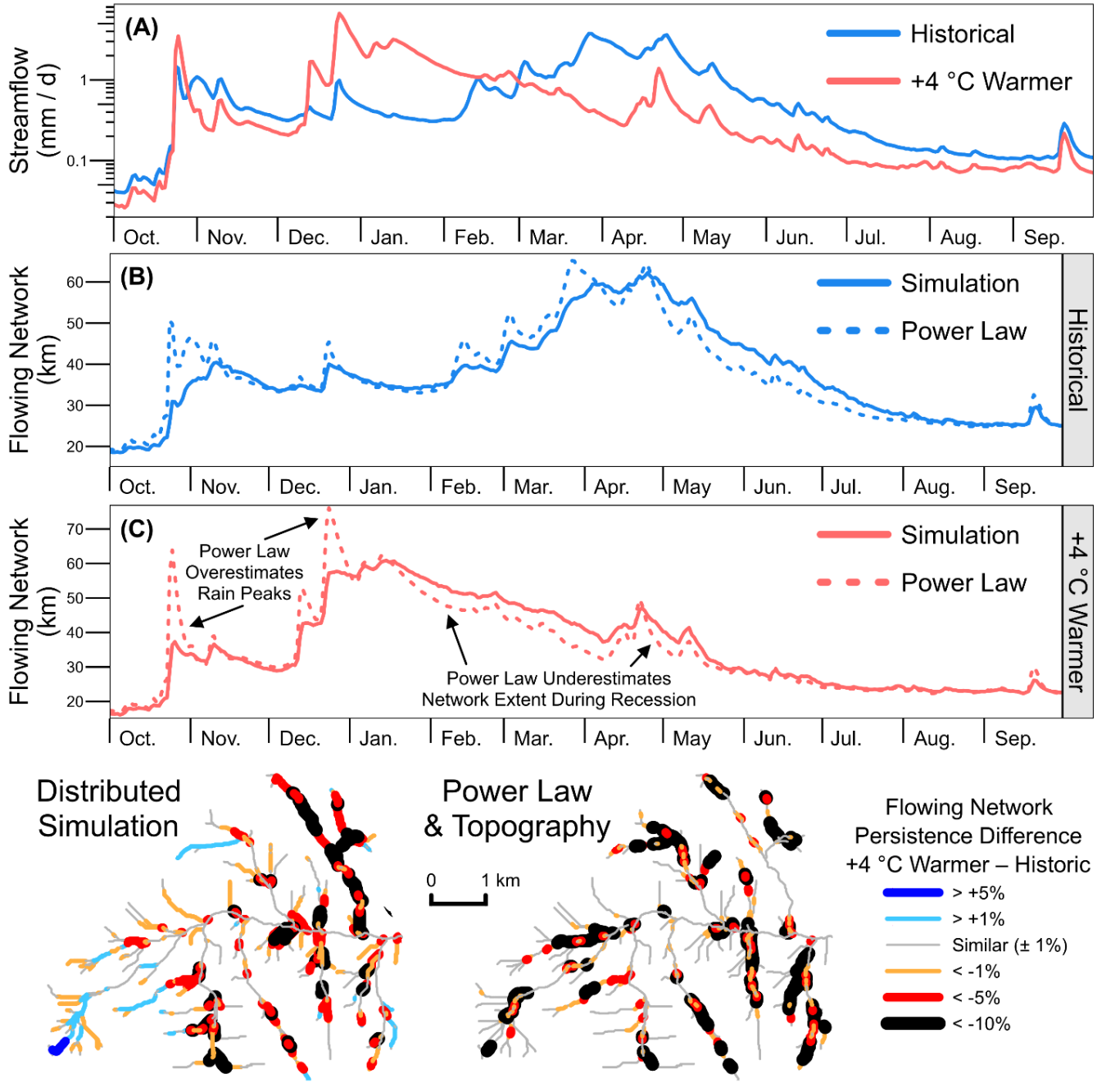

Figure 7. Example timeseries for one year of the simulation under historical or +4 °C warmer climate scenarios, showing (A) simulated streamflow and (B-C) flowing network length simulated directly or estimated from a power law in the historical (B) or warmer (C) scenarios. Maps show the change in streamflow persistence (fraction of flowing days across 24 years) between warmer and historical model simulations (left) or inferred from the combination of a power law and static topographic flow routing assumptions (right).

https://doi.org/10.5194/egusphere-2025-6294
Preprint. Discussion started: 12 January 2026

In the warming scenario, flowing streams become overall less persistent, but static topographic assumptions fail to capture the magnitude—and sometimes even the direction—of DHSVM-predicted climate change effects. The mean decrease in stream persistence (fraction of flowing days) for all stream reaches is 2% ($p < 0.01$), but the persistence of some reaches decreases by as much as 15% or increases by as much as 6% (Fig. 6). We compare these simulation results with a simpler approach based on the power law and a fixed hierarchical ranking (Botter et al. 2021) that distributes L among stream reaches based on the topographic wetness index, analogous to prior L-Q modeling approaches (Beven and Kirkby 1979, Mahoney et al. 2023). This simpler approach predicts the same 2% mean decrease in persistence, but all reaches decrease or remain unchanged (Fig. 7). Moreover, the fixed hierarchical approach leads to a 40% overestimation of the number of reaches with at least a 10% decrease in persistence. A fixed hierarchical approach to streamflow persistence does not account for the potential spatial variability and nonlinearity in the climate sensitivity of different streams. In SCB, the stream reaches with increased persistence in a warmer climate occur at the highest elevations, where earlier snowmelt permits a longer runoff season. We expect that the nonuniformity of interactions between climate and flowing stream networks could be even more pronounced over climate gradients that extend beyond the 700 m elevation range in SCB.

3.5 Relevant Timescales for L-Q Hysteresis

Quantifying the timescales over which GW decouples L and Q is important for understanding whether these effects are relevant for fluvial and riparian processes. The autocorrelation of L at different time lags (in days) provides a metric quantifying the temporal stability of flowing stream networks. At progressively longer lags, the autocorrelation of L_P (estimated by the power law) tends to decrease more rapidly compared to the autocorrelation of L (simulated by DHSVM), indicating that the power law may overestimate the elasticity of the stream network in some circumstances. We define the flowing network "hysteresis effect," HE_L, as the difference in autocorrelation between the timeseries of L simulated by the distributed model or estimated by the power law. Positive HE_L indicates a stronger autocorrelation in L than would be expected from temporal persistence in Q alone, i.e., damped elasticity of L relative to Q. Based on the autocorrelation within 24 yearly bootstrap samples over the historical simulation period (Fig. S12), we find that HE_L is significantly greater than zero at lags of 1-95 days ($p < 0.01$). Across the full 24-year period, the hysteresis effect is largest at a lag of 47 days, at which point the simulation predicts an autocorrelation of 0.60 and the power law predicts an autocorrelation of 0.51 (HE_L = 0.09). An analogous hysteresis effect, HE_{EC}, is detectable in the EC timeseries. An EC-Q power law similarly underestimates the measured EC autocorrelation, but HE_{EC} is only statistically significant at shorter lags of 1-5 days ($p < 0.01$) and 6-7 days ($p < 0.05$), potentially due to measurement noise or confounding sources of EC variability.

Greater rain dominance causes a flashier hydrograph, but DHSVM predicts that GW hysteresis would buffer changes in L (Fig. 7), so the power law approximation increasingly overestimates the sensitivity of the flowing network in the warmer climate relative to DHSVM simulations (Fig. S12). The increase in HE_L between historical and +4 °C simulations is

https://doi.org/10.5194/egusphere-2025-6294
Preprint. Discussion started: 12 January 2026

significant at time lags of 1-36 days ($p < 0.01$). Across the full 23-year period, the change in HE_L is largest at a lag of 9 days, at which point the power law autocorrelation decreases from 0.92 to 0.89 in the warmer climate, while the simulation autocorrelation remains nearly unchanged at 0.96. Although HE_L overall peaks at 47 days, and remains significant beyond three months, the mediating role of hysteresis on a snow-rain transition is most pronounced at much shorter lags, which intuitively matches the shorter hydrological response time after individual storms compared to the longer snowmelt period. The power law matches the DHSVM prediction of reduced below-median network lengths but does not account for an increase in upper-quartile lengths associated with hysteresis after rain (Fig. S13).

The flowing network hysteresis effect (HE_L) is larger in years with reduced snow dominance (Fig. 8). Considering HE_L calculated for 24 bootstrap annual periods in each of the historical and warmer climates, a smaller simulated annual snowfall fraction correlates with a larger hysteresis effect at lags of 10, 20, and 30 days ($r = -0.69, -0.65, -0.52$; $p < 0.01$). Considering just the historical years, the correlation between HE_L and the annual snowfall fraction remain significant at 10, 20, and 30 day lags ($p < 0.01$). Analogously for measured EC data across 15 bootstrap periods, a larger hysteresis effect (HE_{EC}) significantly correlates with a smaller snowfall fraction at lags of 10, 20, and 30 days ($r = -0.61, -0.58, -0.58$; $p < 0.05$). Excluding the two years with negative HE_{EC}, the measured correlation at a 10-day lag rises to $r = -0.65$ ($p < 0.05$). Although the mean value of HE_{EC} itself is not significantly different from zero at lags beyond 7 days, the correlation of HE_{EC} with the snow fraction is significant even at a 30-day lag. This suggests that noise in the EC signal may obscure longer-term hysteresis within individual years, but the month-scale hysteresis effect becomes apparent when comparing across 14 years with different degrees of snow or rain dominance.

https://doi.org/10.5194/egusphere-2025-6294
Preprint. Discussion started: 12 January 2026

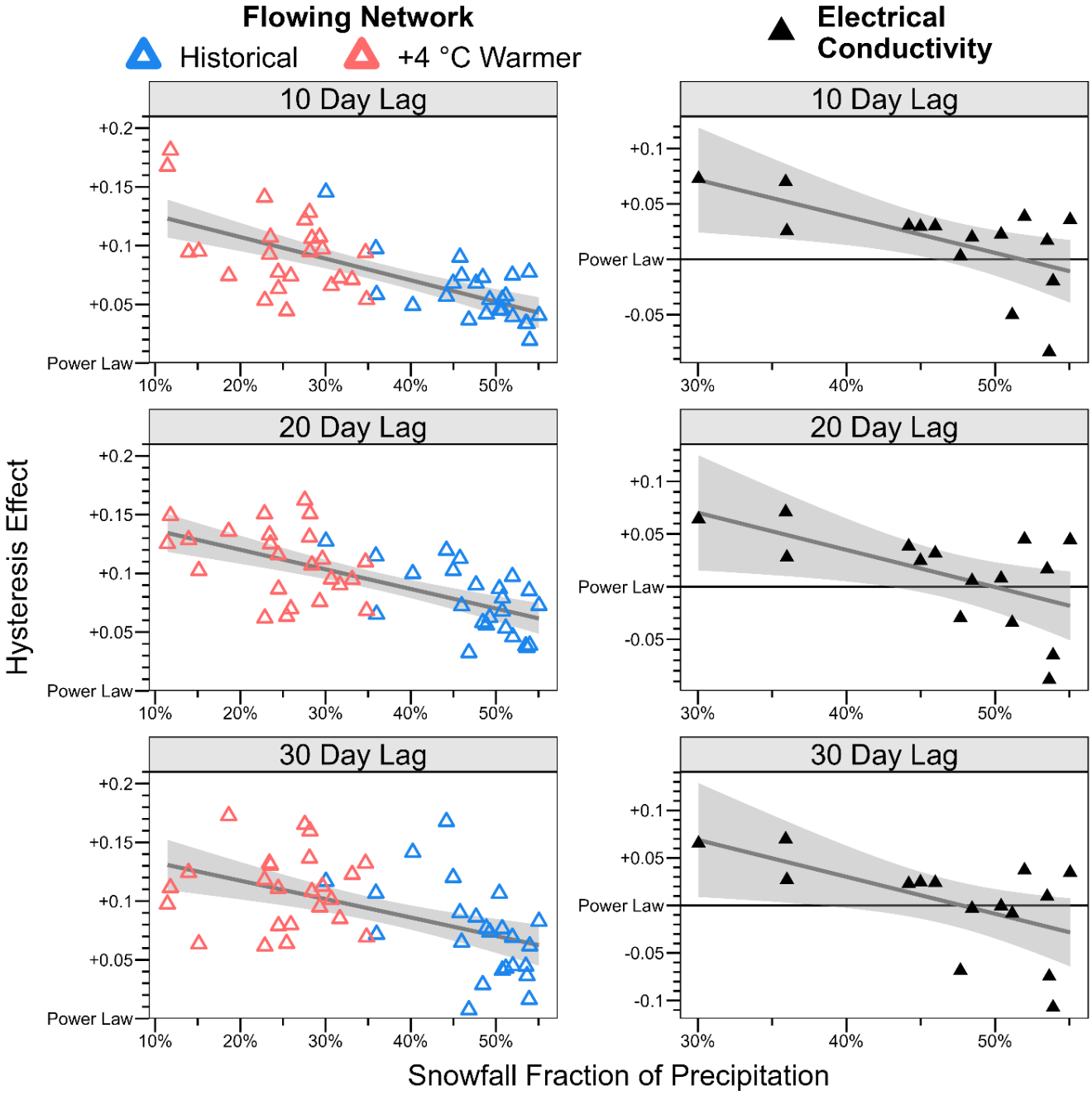

Figure 8. A stronger flowing network hysteresis effect (difference in simulated autocorrelation relative to a power law assumption) is associated with a smaller fraction of precipitation falling as snow. A similar relationship is detected in timeseries of measured stream electrical conductivity, which is related to groundwater age. Shaded gray regions show the 95% confidence range for the best-fit linear trendline.

https://doi.org/10.5194/egusphere-2025-6294
Preprint. Discussion started: 12 January 2026

4 Discussion

Our simulations and water chemistry data support the hypothesis that groundwater (GW) hysteresis partially decouples the flowing stream network length (L) from streamflow (Q) in a headwaters catchment on daily to seasonal timescales, and this decoupling becomes more pronounced in years with relatively less snow and more rain. Model simulations predict that the degree of the hypothesized L-Q decoupling may be surprisingly large: simulated Q can vary by more than 100% at a constant network length, and networks varying by 33% or more can produce the same Q (Fig. 4). Moreover, the hypothesized effect manifests in streams ranging from small trickles to as much as 22% of total streamflow, indicating a substantial reorganization of spatial streamflow generation patterns. A power law approximation, in which L is perfectly coupled to Q, would underestimate the autocorrelation of simulated L variability on daily to >2 month timescales. Put simply, Q is not necessarily a good proxy for L in certain circumstances. Similar power law deviations are detected in observational records from the same watershed. Using measured electrical conductivity as a proxy for solute-rich streamflow derived from slower groundwater flowpaths, the seasonal hysteresis effect diagnosed here provides a physical explanation for why stream chemistry differs between the rising and falling hydrograph limbs at the same streamflow level (Fig. 5). Importantly, our results suggest that nonmonotonicity in the L-Q scaling relationship is likely to be significant over the spatiotemporal timescales that matter for fluvial and riparian biogeochemical processes (Alexander et al. 2007, Meyer et al. 2007, Aufdenkampe et al. 2011, Marx et al. 2017, Liu et al. 2022).

We expect that groundwater hysteresis causes anomalously small flowing networks during autumn and early winter rainfall-runoff events and anomalously large flowing networks during spring and summer snowmelt recession, summarized in Fig. 9. These GW-L-Q hysteresis relationships (Fig. 5) result from the extensively documented spatiotemporal variability of hydraulic gradients and flow directions in response to antecedent conditions (e.g., McGlynn et al. 2004, Detty and McGuire 2010, Rodhe and Seibert 2011, von Freyberg et al. 2014). As the catchment “wets up” after the growing season, streamflow rises rapidly due to decreased riparian evapotranspiration and steepening hydraulic gradients during early winter storms. However, raising the catchment-average GW level (which controls stream network expansion) requires a substantial increase in the spatially distributed dynamic water storage, which is accumulated over time. Conversely, as GW declines during recession, valley-bottom hydraulic gradients become increasingly parallel to streams, reducing channel inflow (Rodhe and Seibert 2011, van Meerveld et al. 2015). Flowing streams can persist “on top” of the receding water table even if inflow from GW to Q is minimal. Hence, catchment-average GW and L both lag Q (Fig. 5).

https://doi.org/10.5194/egusphere-2025-6294
Preprint. Discussion started: 12 January 2026

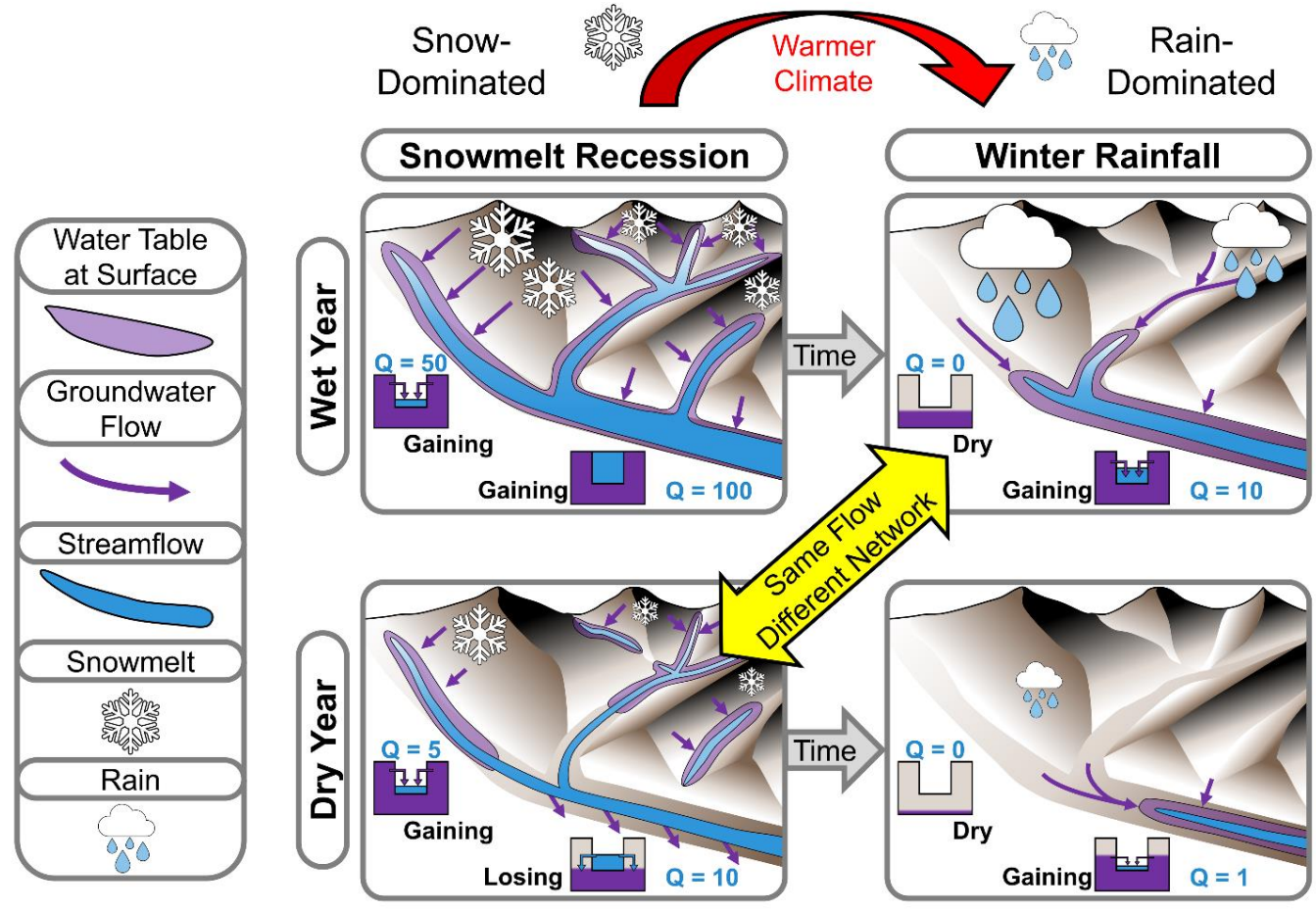

Figure 9. Revised conceptual model of stream-groundwater interactions in a mountain catchment, illustrating the emergence of stream network hysteresis caused by transient groundwater flow between hillslopes and riparian zones. Contrast with conceptual model illustrated in Fig. 7 of Godsey and Kirchner (2014), which assumes equilibrium groundwater flow. Channel cross-sections show how this conceptual model is simulated at the grid scale (cf. schematic in Fig. S1). Antecedent groundwater priming from snowmelt and rain activates a relatively large flowing stream network during the seasonal recession period, but rainfall during periods with a low antecedent water table can cause a rapid increase in streamflow even though the flowing network remains small. In a warmer climate, winter rainfall becomes more dominant than spring snowmelt, altering the spatial configuration of streamflow generation and flowing network connectivity.

Measured hysteresis in the stream EC-Q relationship supports our interpretation of GW-L-Q hysteresis on daily to seasonal timescales (Figs. 5-6). Chemical weathering of the underlying volcanic bedrock in SCB creates a positive correlation between EC and GW residence time, as measured by multiple geochemical tracers across springs of varying age (Rademacher et al. 2001). Additional observations across other Sierra Nevada catchments of varying lithology show that longer flowpaths and older GW sources similarly tend to have higher EC (Holloway and Dahlgren 2001, Ahearn et al. 2004, Meyers et al. 2022). The daily EC measurements in SCB reveal that stream EC remains elevated as Q begins to rise, interpreted as an outsized contribution from riparian aquifers connected to relatively long valley-bottom GW flowpaths with

https://doi.org/10.5194/egusphere-2025-6294
Preprint. Discussion started: 12 January 2026

longer residence times. Conversely, stream EC remains suppressed during the falling hydrograph limb as Q decreases, consistent with the transient activation of relatively fast, shallow, chemically depleted GW flowpaths in hillslope and headwater regions. Notably, the hysteresis effect in EC (HE_{EC}) is significantly positive at short time lags of 1-7 days and its inverse correlation with the annual snowfall fraction remains significant even at time lags of 30 days (Fig. 7). This behavior suggests that EC may record not only event-scale runoff dynamics, but also broader seasonal GW memory effects. In more rain-dominated years, stream EC is relatively stable compared to a power law relationship with streamflow, possibly reflecting inputs from older, slowly responding GW sources after each rainfall-runoff event. Together, these findings suggest that EC, and by extension other geochemical tracers of GW residence times (Marcais et al. 2018, Druhan and Benettin 2023), could be useful complementary proxies for detecting shifts in GW ages under changing climate conditions. Moreover, these observations further support our model-based hypothesis that GW hysteresis will become more important for mediating the flowing stream network as rain replaces snow, even on monthly timescales. The volcanic lithology of our SCB study area is particularly notable for the importance of old GW (e.g., Rademacher et al. 2005), and catchments with different subsurface characteristics may have weaker or stronger L-Q hysteresis, which might be detectable though analysis of EC-Q relationships.

Our simulations predict that a partial shift from snowmelt-driven to rainfall-driven runoff generation would heighten the importance of GW hysteresis as a mediator of flowing network length (Fig. 9). Compared to the distributed simulation model, a power law approximation overestimates L during storm runoff events when the watershed is dry and GW is concentrated in higher-order convergence zones (Figs. 2-3). Conversely, the power law approximation consistently underestimates simulated L during seasonal recession when GW is distributed more evenly throughout the catchment (Figs. 2-3). Although both types of biases are present in both simulated climate scenarios (Fig. 7), the recession underestimation becomes relatively less important with a declining snowmelt season, and the storm peak overestimation becomes relatively more important with increasing cold-season rainfall-runoff events.

Flowing stream network studies may need to account for the pervasive hysteretic character of hydrological storage and runoff generation processes to avoid systematically biased predictions of change. Hysteresis is an emergent property of threshold-like behavior in hydrological systems, and this recognition heralds a “paradigm shift” in conceptual models of streamflow generation (Spence 2010). Still, hysteresis is missing from the widely accepted conceptual model of flowing stream network dynamics (Godsey and Kirchner 2014, Prancevic et al. 2025) and likewise ignored by most prior mechanistic simulations (Ward et al. 2018, Gao et al. 2021, Mahoney et al. 2023). Although our fully dynamic simulations are limited to one watershed, our conceptual model (Fig. 9) is generalizable to other mountain headwaters catchments where GW mediates streamflow generation. Anecdotally, we observe similar seasonal EC hysteresis signals in other watersheds, especially in groundwater-dominated basins with volcanic lithologies such as the Madison River in Yellowstone National Park, Wyoming, USA (Gardner et al. 2010, McCleskey et al. 2012), though a comprehensive multi-basin investigation is beyond

https://doi.org/10.5194/egusphere-2025-6294
Preprint. Discussion started: 12 January 2026

the scope of the current study. Future research could investigate the variability of EC as a proxy for L-Q hysteresis across multiple catchments to constrain the role of topography, lithology, land surface cover, and climate. Our model results indicate that L-Q hysteresis may be nonnegligible at scales ranging from first-order headwaters stream reaches up to the 27 km^2 SCB catchment, and future simulations could quantify this effect at even larger watershed scales. Finally, long-term spatially explicit monitoring of stream networks could validate or refine our understanding of the relevant time lags and predicted changes in L-Q hysteresis, though such monitoring may be unrealistic given the many-year timescales and daily sampling frequencies required to quantify the hysteresis effect (HE_L) defined here.

5 Conclusions

Our model simulations suggest a new process-based hypothesis (non-equilibrium groundwater flow) to explain observed seasonal hysteresis in both stream chemistry and flowing network length. Process-based hydrological models have been criticized as overparameterized and merely representing what we already know about hydrology, and Kirchner (2006) claims that "all hydrological knowledge ultimately comes from observations, experiments, and measurements." The present study seems to offer a counterexample, wherein a "bottom-up" approach based on microscale physics yields a novel hypothesis about catchment-scale hydrological behavior. While field surveys provide valuable insight into the first-order behavior of dynamic stream networks, the second-order hysteresis effect diagnosed here only becomes quantifiable from thousands of simulated daily stream network maps, a dataset that would require a monumental effort to collect in the field. A related groundwater hysteresis signal in measured stream geochemical timeseries supports our findings, but the connection to channel dynamics is not quantifiable from existing measurements alone. At the outset of this study, we merely sought to reproduce known stream network dynamics (i.e., expansion/contraction/disconnection) using simple physically based rules (Fig. S1), but the presence of substantial scatter in the simulated scaling relationship (Fig. 3) prompted us to investigate power law anomalies for both stream chemistry and network length, ultimately leading to our hypothesis of a groundwater hysteresis effect (Fig. 5). The emergence of complexity from the repeated application of simple rules is perhaps one of the most surprising results of computational science (Conway and Gardner 1970, Wolfram 1984, Cook 2004), especially when those rules are grounded in physical constraints like the dynamic groundwater flow directions in this study (Fig. S1).

A physically based, spatially distributed surface-groundwater interaction scheme enables investigation of potential climate change effects and other disturbances. Approaches based purely on past observations (such as the L-Q power law and typical machine learning methods) are untested in out-of-sample conditions by definition, so these purely empirical approaches are problematic for investigations of nonstationarity (e.g., climate change and land surface disturbance). Compared to the power law approximation, a distributed simulation yields different predictions of the magnitude, and even the directionality, of climate-induced stream network changes (Fig. 7). While incorporating missing processes into models is obviously worthwhile in its own right, model experiments with sufficient space for emergent complexity may also suggest revised

https://doi.org/10.5194/egusphere-2025-6294
Preprint. Discussion started: 12 January 2026

conceptual models (Fig. 9) that motivate new data collection or novel interpretations of existing field data. Additional iterative model and field investigations are needed to further test and refine our understanding of stream network dynamics in nonstationary environments.

Code and Data Availability

All processing scripts, model code, and data needed to reproduce the results and figures are archived at https://doi.org/10.5281/zenodo.17958145 (Boardman 2025).

Video Supplement

The video supplement, consisting of a groundwater flow and active stream network animation from the DHSVM simulations, is available online at TIB AV-PORTAL per Copernicus Publications instructions, but is not yet available because it has not been issued a DOI. During review, the video supplement can be accessed online at https://mountainhydrology.com/sagehen_groundwater_stream_animation/.

Author Contribution

ENB developed the model code modifications, implemented the simulations and analysis, created the figures, and wrote the initial manuscript. MSW, NMF, JAW, and AAH each contributed to conceptualization, validation, and manuscript editing. AAH additionally contributed to supervision and funding acquisition.

Competing Interests

At least one of the (co-)authors is a member of the editorial board of *Hydrology and Earth System Sciences*. The authors have no other competing interests to declare.

Financial Support

This research has been supported by the National Science Foundation Graduate Research Fellowship Program (grant no. 1937966) and the National Science Foundation Division of Earth Sciences (grant nos. EAR 2012310, EAR 2012188, and EAR 2308548).

https://doi.org/10.5194/egusphere-2025-6294
Preprint. Discussion started: 12 January 2026

References

Abatzoglou, J. T.: Development of gridded surface meteorological data for ecological applications and modelling, International Journal of Climatology, 33, 121–131, https://doi.org/10.1002/joc.3413, 2013.

Ahearn, D. S., Sheibley, R. W., Dahlgren, R. A., and Keller, K. E.: Temporal dynamics of stream water chemistry in the last free-flowing river draining the western Sierra Nevada, California, Journal of Hydrology, 295, 47–63, https://doi.org/10.1016/j.jhydrol.2004.02.016, 2004.

Alexander, R. B., Boyer, E. W., Smith, R. A., Schwarz, G. E., and Moore, R. B.: The Role of Headwater Streams in Downstream Water Quality, JAWRA Journal of the American Water Resources Association, 43, 41–59, https://doi.org/10.1111/j.1752-1688.2007.00005.x, 2007.

Allan, J. D., Castillo, M. M., and Capps, K. A.: Stream Ecology: Structure and Function of Running Waters, Springer Nature, 494 pp., 2021.

Allen, D. M., Whitfield, P. H., and Werner, A.: Groundwater level responses in temperate mountainous terrain: regime classification, and linkages to climate and streamflow, Hydrological Processes, 24, 3392–3412, https://doi.org/10.1002/hyp.7757, 2010.

Andermann, C., Longuevergne, L., Bonnet, S., Crave, A., Davy, P., and Gloaguen, R.: Impact of transient groundwater storage on the discharge of Himalayan rivers, Nature Geosci, 5, 127–132, https://doi.org/10.1038/ngeo1356, 2012.

Aufdenkampe, A. K., Mayorga, E., Raymond, P. A., Melack, J. M., Doney, S. C., Alin, S. R., Aalto, R. E., and Yoo, K.: Riverine coupling of biogeochemical cycles between land, oceans, and atmosphere, Frontiers in Ecology and the Environment, 9, 53–60, https://doi.org/10.1890/100014, 2011.

Beckers, J., Smerdon, B., Redding, T., Anderson, A., Pike, R., and Werner, A. T.: Hydrologic models for forest management applications. Part 1: Model selection, Streamline Watershed Management Bulletin, 13, 2009.

Bennett, A., Hamman, J., and Nijssen, B.: MetSim: A Python package for estimation and disaggregation of meteorological data, JOSS, 5, 2042, https://doi.org/10.21105/joss.02042, 2020.

Berghuijs, W. R., Woods, R. A., and Hrachowitz, M.: A precipitation shift from snow towards rain leads to a decrease in streamflow, Nature Clim Change, 4, 583–586, https://doi.org/10.1038/nclimate2246, 2014.

Beven, K.: On subsurface stormflow: Predictions with simple kinematic theory for saturated and unsaturated flows, Water Resources Research, 18, 1627–1633, https://doi.org/10.1029/WR018i006p01627, 1982.

Beven, K.: Searching for the Holy Grail of scientific hydrology: Q_t=(S, R, Δt)A as closure, Hydrology and Earth System Sciences, 10, 609–618, https://doi.org/10.5194/hess-10-609-2006, 2006.

Beven, K. J. and Kirkby, M. J.: A physically based, variable contributing area model of basin hydrology / Un modèle à base physique de zone d'appel variable de l'hydrologie du bassin versant, Hydrological Sciences Bulletin, 24, 43–69, https://doi.org/10.1080/02626667909491834, 1979.

https://doi.org/10.5194/egusphere-2025-6294
Preprint. Discussion started: 12 January 2026

Bieger, K., Rathjens, H., Allen, P. M., and Arnold, J. G.: Development and Evaluation of Bankfull Hydraulic Geometry Relationships for the Physiographic Regions of the United States, JAWRA Journal of the American Water Resources Association, 51, 842–858, https://doi.org/10.1111/jawr.12282, 2015.

Blumhagen, E. D. and Clark, J. F.: Carbon sources and signals through time in an Alpine groundwater Basin, Sagehen California, Applied Geochemistry, 23, 2284–2291, https://doi.org/10.1016/j.apgeochem.2008.03.010, 2008.

Boardman, E.: Data and Code for Stream Network Hysteresis Study Using DHSVM in Sagehen Creek Basin, https://doi.org/10.5281/zenodo.17958146, 2025.

Boardman, E. N., Boisramé, G. F. S., Wigmosta, M. S., Shriver, R. K., and Harpold, A. A.: Improving model calibrations in a changing world: controlling for nonstationarity after mega disturbance reduces hydrological uncertainty, Hydrol. Earth Syst. Sci., 29, 6333–6352, https://doi.org/10.5194/hess-29-6333-2025, 2025.

Botter, G., Vingiani, F., Senatore, A., Jensen, C., Weiler, M., McGuire, K., Mendicino, G., and Durighetto, N.: Hierarchical climate-driven dynamics of the active channel length in temporary streams, Sci Rep, 11, 21503, https://doi.org/10.1038/s41598-021-00922-2, 2021.

Breiman, L., Cutler, A., Liaw, A., and Wiener, M.: randomForest: Breiman and Cutlers Random Forests for Classification and Regression [software], https://doi.org/10.32614/CRAN.package.randomForest, 2002.

Brown, L. E., Milner, A. M., and Hannah, D. M.: Groundwater influence on alpine stream ecosystems, Freshwater Biology, 52, 878–890, https://doi.org/10.1111/j.1365-2427.2007.01739.x, 2007.

Camporese, M., Penna, D., Borga, M., and Paniconi, C.: A field and modeling study of nonlinear storage-discharge dynamics for an Alpine headwater catchment, Water Resources Research, 50, 806–822, https://doi.org/10.1002/2013WR013604, 2014.

Cano-Paoli, K., Chiogna, G., and Bellin, A.: Convenient use of electrical conductivity measurements to investigate hydrological processes in Alpine headwaters, Science of The Total Environment, 685, 37–49, https://doi.org/10.1016/j.scitotenv.2019.05.166, 2019.

Carlston, C. W.: Drainage Density and Streamflow, U.S. Government Printing Office, 20 pp., 1963.

Castro, J. M. and Thorne, C. R.: The stream evolution triangle: Integrating geology, hydrology, and biology, River Research and Applications, 35, 315–326, https://doi.org/10.1002/rra.3421, 2019.

Clark, M. P. and Kavetski, D.: Ancient numerical daemons of conceptual hydrological modeling: 1. Fidelity and efficiency of time stepping schemes, Water Resources Research, 46, https://doi.org/10.1029/2009WR008894, 2010.

Clarke, A., Mac Nally, R., Bond, N., and Lake, P. S.: Macroinvertebrate diversity in headwater streams: a review, Freshwater Biology, 53, 1707–1721, https://doi.org/10.1111/j.1365-2427.2008.02041.x, 2008.

Conway, J. and Gardner, M.: Mathematical Games, Scientific American, 223, 120–123, 1970.

Cook, M.: Universality in Elementary Cellular Automata, ComplexSystems, 15, 1–40, https://doi.org/10.25088/ComplexSystems.15.1.1, 2004.

https://doi.org/10.5194/egusphere-2025-6294
Preprint. Discussion started: 12 January 2026

Cristea, N. C., Lundquist, J. D., Loheide, S. P., Lowry, C. S., and Moore, C. E.: Modelling how vegetation cover affects climate change impacts on streamflow timing and magnitude in the snowmelt-dominated upper Tuolumne Basin, Sierra Nevada, Hydrological Processes, 28, 3896–3918, https://doi.org/10.1002/hyp.9909, 2014.

De Vries, J. J.: Seasonal expansion and contraction of stream networks in shallow groundwater systems, Journal of Hydrology, 170, 15–26, https://doi.org/10.1016/0022-1694(95)02684-H, 1995.

Detty, J. M. and McGuire, K. J.: Threshold changes in storm runoff generation at a till-mantled headwater catchment, Water Resources Research, 46, https://doi.org/10.1029/2009WR008102, 2010a.

Detty, J. M. and McGuire, K. J.: Topographic controls on shallow groundwater dynamics: implications of hydrologic connectivity between hillslopes and riparian zones in a till mantled catchment, Hydrological Processes, 24, 2222–2236, https://doi.org/10.1002/hyp.7656, 2010b.

Dewitz, J. and U.S. Geological Survey: National Land Cover Database (NLCD) 2019 Products [data set], https://doi.org/10.5066/P9JZ7AO3, 2019.

Dhungel, S., Tarboton, D. G., Jin, J., and Hawkins, C. P.: Potential Effects of Climate Change on Ecologically Relevant Streamflow Regimes: Climate Change and Streamflow Regimes, River Res. Applic., 32, 1827–1840, https://doi.org/10.1002/rra.3029, 2016.

Downing, J. A., Cole ,J.J., Duarte ,C.M., Middelburg ,J.J., Melack ,J.M., Prairie ,Y.T., Kortelainen ,P., Striegl ,R.G., McDowell ,W.H., and and Tranvik, L. J.: Global abundance and size distribution of streams and rivers, Inland Waters, 2, 229–236, https://doi.org/10.5268/IW-2.4.502, 2012.

Dralle, D. N., Lapides, D. A., Rempe, D. M., and Hahm, W. J.: Mapping Surface Water Presence and Hyporheic Flow Properties of Headwater Stream Networks With Multispectral Satellite Imagery, Water Resources Research, 59, e2022WR034169, https://doi.org/10.1029/2022WR034169, 2023.

Druhan, J. L. and Benettin, P.: Isotope Ratio – Discharge Relationships of Solutes Derived From Weathering Reactions, American Journal of Science, 323, https://doi.org/10.2475/001c.84469, 2023.

Dugdale, S. J., Klaus, J., and Hannah, D. M.: Looking to the Skies: Realising the Combined Potential of Drones and Thermal Infrared Imagery to Advance Hydrological Process Understanding in Headwaters, Water Resources Research, 58, e2021WR031168, https://doi.org/10.1029/2021WR031168, 2022.

Durighetto, N., Vingiani, F., Bertassello, L. E., Camporese, M., and Botter, G.: Intraseasonal Drainage Network Dynamics in a Headwater Catchment of the Italian Alps, Water Resources Research, 56, e2019WR025563, https://doi.org/10.1029/2019WR025563, 2020.

Essaid, H. I. and Hill, B. R.: Watershed-scale modeling of streamflow change in incised montane meadows, Water Resources Research, 50, 2657–2678, https://doi.org/10.1002/2013WR014420, 2014.

Foster, L. M., Bearup, L. A., Molotch, N. P., Brooks, P. B., and Maxwell, R. M.: Energy budget increases reduce mean streamflow more than snow–rain transitions: using integrated modeling to isolate climate change impacts on Rocky Mountain hydrology, Environ. Res. Lett., 11, 044015, https://doi.org/10.1088/1748-9326/11/4/044015, 2016.

https://doi.org/10.5194/egusphere-2025-6294
Preprint. Discussion started: 12 January 2026

Freeman, M. C., Pringle, C. M., and Jackson, C. R.: Hydrologic Connectivity and the Contribution of Stream Headwaters to Ecological Integrity at Regional Scales, JAWRA Journal of the American Water Resources Association, 43, 5–14, https://doi.org/10.1111/j.1752-1688.2007.00002.x, 2007.

Freeze, R. A. and Cherry, J. A.: Groundwater, Prentice-Hall, Englewood Cliffs, N.J, 604 pp., 1979.

von Freyberg, J., Radny, D., Gall, H. E., and Schirmer, M.: Implications of hydrologic connectivity between hillslopes and riparian zones on streamflow composition, Journal of Contaminant Hydrology, 169, 62–74, https://doi.org/10.1016/j.jconhyd.2014.07.005, 2014.

Fritz, K. M., Hagenbuch, E., D'Amico, E., Reif, M., Wigington, P. J., Leibowitz, S. G., Comeleo, R. L., Ebersole, J. L., and Nadeau, T.: Comparing the Extent and Permanence of Headwater Streams From Two Field Surveys to Values From Hydrographic Databases and Maps, J American Water Resour Assoc, 49, 867–882, https://doi.org/10.1111/jawr.12040, 2013.

Gao, S., Chen, M., Li, Z., Cook, S., Allen, D., Neeson, T., Yang, T., Yami, T., and Hong, Y.: Mapping dynamic non-perennial stream networks using high-resolution distributed hydrologic simulation: A case study in the upper blue river basin, Journal of Hydrology, 600, 126522, https://doi.org/10.1016/j.jhydrol.2021.126522, 2021.

Godsey, S. E. and Kirchner, J. W.: Dynamic, discontinuous stream networks: hydrologically driven variations in active drainage density, flowing channels and stream order, Hydrological Processes, 28, 5791–5803, https://doi.org/10.1002/hyp.10310, 2014.

Gordon, B. L., Brooks, P. D., Krogh, S. A., Boisrame, G. F. S., Carroll, R. W. H., McNamara, J. P., and Harpold, A. A.: Why does snowmelt-driven streamflow response to warming vary? A data-driven review and predictive framework, Environ. Res. Lett., 17, 053004, https://doi.org/10.1088/1748-9326/ac64b4, 2022.

Graup, L. J., Tague, C. L., Harpold, A. A., and Krogh, S. A.: Subsurface Lateral Flows Buffer Riparian Water Stress Against Snow Drought, Journal of Geophysical Research: Biogeosciences, 127, e2022JG006980, https://doi.org/10.1029/2022JG006980, 2022.

Gregory, K. J. and Walling, D. E.: The variation of drainage density within a catchment, International Association of Scientific Hydrology. Bulletin, 13, 61–68, https://doi.org/10.1080/02626666809493583, 1968.

Gu, H., Xu, Y.-P., Liu, L., Xie, J., Wang, L., Pan, S., and Guo, Y.: Seasonal catchment memory of high mountain rivers in the Tibetan Plateau, Nat Commun, 14, 3173, https://doi.org/10.1038/s41467-023-38966-9, 2023.

Gupta, S., Papritz, A., Lehmann, P., Hengl, T., Bonetti, S., and Or, D.: Global Mapping of Soil Water Characteristics Parameters— Fusing Curated Data with Machine Learning and Environmental Covariates, Remote Sensing, 14, 1947, https://doi.org/10.3390/rs14081947, 2022.

Harpold, A. A. and Molotch, N. P.: Sensitivity of soil water availability to changing snowmelt timing in the western U.S., Geophysical Research Letters, 42, 8011–8020, https://doi.org/10.1002/2015GL065855, 2015.

https://doi.org/10.5194/egusphere-2025-6294
Preprint. Discussion started: 12 January 2026

Hasan, M. M., Strong, C., Brooks, P. D., Burian, S. J., and Barber, M. E.: Quantifying climate change impacts on low flows of small high mountain watersheds: A nonstationary approach, Journal of Hydrology: Regional Studies, 48, 101463, https://doi.org/10.1016/j.ejrh.2023.101463, 2023.

Hewlett, J. D. and Hibbert, A. R.: Factors affecting the response of small watersheds to precipitation in humid areas, Forest Hydrology, 11, 275–290, 1967.

Holloway, J. M. and Dahlgren, R. A.: Seasonal and event-scale variations in solute chemistry for four Sierra Nevada catchments, Journal of Hydrology, 250, 106–121, https://doi.org/10.1016/S0022-1694(01)00424-3, 2001.

Hrachowitz, M. and Clark, M. P.: HESS Opinions: The complementary merits of competing modelling philosophies in hydrology, Hydrology and Earth System Sciences, 21, 3953–3973, https://doi.org/10.5194/hess-21-3953-2017, 2017.

Huang, X., Hall, A. D., and Berg, N.: Anthropogenic Warming Impacts on Today's Sierra Nevada Snowpack and Flood Risk, Geophysical Research Letters, 45, 6215–6222, https://doi.org/10.1029/2018GL077432, 2018.

Jaeger, K. L., Olden, J. D., and Pelland, N. A.: Climate change poised to threaten hydrologic connectivity and endemic fishes in dryland streams, Proceedings of the National Academy of Sciences, 111, 13894–13899, https://doi.org/10.1073/pnas.1320890111, 2014.

Jensen, C. K., McGuire, K. J., and Prince, P. S.: Headwater stream length dynamics across four physiographic provinces of the Appalachian Highlands, Hydrological Processes, 31, 3350–3363, https://doi.org/10.1002/hyp.11259, 2017.

Jensen, C. K., McGuire, K. J., McLaughlin, D. L., and Scott, D. T.: Quantifying spatiotemporal variation in headwater stream length using flow intermittency sensors, Environ Monit Assess, 191, 226, https://doi.org/10.1007/s10661-019-7373-8, 2019.

Jones, D. R., Schonlau, M., and Welch, W. J.: Efficient Global Optimization of Expensive Black-Box Functions, Journal of Global Optimization, 13, 455–492, https://doi.org/10.1023/A:1008306431147, 1998.

Kampf, S. K. and Lefsky, M. A.: Transition of dominant peak flow source from snowmelt to rainfall along the Colorado Front Range: Historical patterns, trends, and lessons from the 2013 Colorado Front Range floods, Water Resources Research, 52, 407–422, https://doi.org/10.1002/2015WR017784, 2016.

Kampf, S. K., Faulconer, J., Shaw, J. R., Sutfin, N. A., and Cooper, D. J.: Rain and channel flow supplements to subsurface water beneath hyper-arid ephemeral stream channels, Journal of Hydrology, 536, 524–533, https://doi.org/10.1016/j.jhydrol.2016.03.016, 2016.

Kendall, K. A., Shanley, J. B., and McDonnell, J. J.: A hydrometric and geochemical approach to test the transmissivity feedback hypothesis during snowmelt, Journal of Hydrology, 219, 188–205, https://doi.org/10.1016/S0022-1694(99)00059-1, 1999.

Kirchner, J. W.: Getting the right answers for the right reasons: Linking measurements, analyses, and models to advance the science of hydrology, Water Resources Research, 42, https://doi.org/10.1029/2005WR004362, 2006.

Kirchner, J. W., Godsey, S. E., Solomon, M., Osterhuber, R., McConnell, J. R., and Penna, D.: The pulse of a montane ecosystem: coupling between daily cycles in solar flux, snowmelt, transpiration, groundwater, and streamflow at

https://doi.org/10.5194/egusphere-2025-6294
Preprint. Discussion started: 12 January 2026

Sagehen Creek and Independence Creek, Sierra Nevada, USA, Hydrology and Earth System Sciences, 24, 5095–5123, https://doi.org/10.5194/hess-24-5095-2020, 2020.

Klos, P. Z., Link, T. E., and Abatzoglou, J. T.: Extent of the rain-snow transition zone in the western U.S. under historic and projected climate, Geophysical Research Letters, 41, 4560–4568, https://doi.org/10.1002/2014GL060500, 2014.

La Barbera, P. and Rosso, R.: On the fractal dimension of stream networks, Water Resources Research, 25, 735–741, https://doi.org/10.1029/WR025i004p00735, 1989.

LANDFIRE: LANDFIRE 2022 Existing Vegetation Type (EVT) [data set], 2022.

Lapides, D. A., Leclerc, C. D., Moidu, H., Dralle, D. N., and Hahm, W. J.: Variability of stream extents controlled by flow regime and network hydraulic scaling, Hydrological Processes, 35, e14079, https://doi.org/10.1002/hyp.14079, 2021.

Lee, S.-Y., Fullerton, A. H., Sun, N., and Torgersen, C. E.: Projecting spatiotemporally explicit effects of climate change on stream temperature: A model comparison and implications for coldwater fishes, Journal of Hydrology, 588, 125066, https://doi.org/10.1016/j.jhydrol.2020.125066, 2020.

Limerinos, J. T.: Determination of the manning coefficient from measured bed roughness in natural channels, U.S. Geological Survey, https://doi.org/10.3133/wsp1898B, 1970.

Liu, S., Kuhn, C., Amatulli, G., Aho, K., Butman, D. E., Allen, G. H., Lin, P., Pan, M., Yamazaki, D., Brinkerhoff, C., Gleason, C., Xia, X., and Raymond, P. A.: The importance of hydrology in routing terrestrial carbon to the atmosphere via global streams and rivers, Proceedings of the National Academy of Sciences, 119, e2106322119, https://doi.org/10.1073/pnas.2106322119, 2022.

Lundquist, J. D. and Cayan, D. R.: Surface temperature patterns in complex terrain: Daily variations and long-term change in the central Sierra Nevada, California, Journal of Geophysical Research: Atmospheres, 112, https://doi.org/10.1029/2006JD007561, 2007.

Mahoney, D. T., Christensen, J. R., Golden, H. E., Lane, C. R., Evenson, G. R., White, E., Fritz, K. M., D'Amico, E., Barton, C. D., Williamson, T. N., Sena, K. L., and Agouridis, C. T.: Dynamics of streamflow permanence in a headwater network: Insights from catchment-scale model simulations, Journal of Hydrology, 620, 129422, https://doi.org/10.1016/j.jhydrol.2023.129422, 2023.

Mandelbrot, B. B.: The fractal geometry of nature, Updated and augmented, 18. print., Freeman, New York, 468 pp., 1999.

Manning, A. H., Clark, J. F., Diaz, S. H., Rademacher, L. K., Earman, S., and Niel Plummer, L.: Evolution of groundwater age in a mountain watershed over a period of thirteen years, Journal of Hydrology, 460–461, 13–28, https://doi.org/10.1016/j.jhydrol.2012.06.030, 2012.

Marçais, J., Gauvain, A., Labasque, T., Abbott, B. W., Pinay, G., Aquilina, L., Chabaux, F., Viville, D., and De Dreuzy, J.-R.: Dating groundwater with dissolved silica and CFC concentrations in crystalline aquifers, Science of The Total Environment, 636, 260–272, https://doi.org/10.1016/j.scitotenv.2018.04.196, 2018.

https://doi.org/10.5194/egusphere-2025-6294
Preprint. Discussion started: 12 January 2026

Marx, A., Dusek, J., Jankovec, J., Sanda, M., Vogel, T., van Geldern, R., Hartmann, J., and Barth, J. a. C.: A review of CO2 and associated carbon dynamics in headwater streams: A global perspective, Reviews of Geophysics, 55, 560–585, https://doi.org/10.1002/2016RG000547, 2017.

McCleskey, R. B., Clor, L. E., Lowenstern, J. B., Evans, W. C., Nordstrom, D. K., Heasler, H., and Huebner, M. A.: Solute and geothermal flux monitoring using electrical conductivity in the Madison, Firehole, and Gibbon Rivers, Yellowstone National Park, Applied Geochemistry, 27, 2370–2381, https://doi.org/10.1016/j.apgeochem.2012.07.019, 2012.

McGlynn, B. L. and McDonnell, J. J.: Quantifying the relative contributions of riparian and hillslope zones to catchment runoff, Water Resources Research, 39, https://doi.org/10.1029/2003WR002091, 2003.

McGlynn, B. L., McDonnell, J. J., Seibert, J., and Kendall, C.: Scale effects on headwater catchment runoff timing, flow sources, and groundwater-streamflow relations, Water Resources Research, 40, https://doi.org/10.1029/2003WR002494, 2004.

van Meerveld, H. J., Seibert, J., and Peters, N. E.: Hillslope–riparian-stream connectivity and flow directions at the Panola Mountain Research Watershed, Hydrological Processes, 29, 3556–3574, https://doi.org/10.1002/hyp.10508, 2015.

Meyer, J. L., Strayer, D. L., Wallace, J. B., Eggert, S. L., Helfman, G. S., and Leonard, N. E.: The Contribution of Headwater Streams to Biodiversity in River Networks[1], J American Water Resour Assoc, 43, 86–103, https://doi.org/10.1111/j.1752-1688.2007.00008.x, 2007.

Meyers, Z. P., Rademacher, L. K., Frisbee, M. D., and Warix, S. R.: Extending classical geochemical weathering studies through the mountain block: The effect of increasing scale on geochemical evolution in the Sierra Nevada (CA), Chemical Geology, 598, 120831, https://doi.org/10.1016/j.chemgeo.2022.120831, 2022.

Null, S. E., Viers, J. H., and Mount, J. F.: Hydrologic Response and Watershed Sensitivity to Climate Warming in California's Sierra Nevada, PLOS ONE, 5, e9932, https://doi.org/10.1371/journal.pone.0009932, 2010.

Patterson, N. K., Lane, B. A., Sandoval-Solis, S., Persad, G. G., and Ortiz-Partida, J. P.: Projected Effects of Temperature and Precipitation Variability Change on Streamflow Patterns Using a Functional Flows Approach, Earth's Future, 10, e2021EF002631, https://doi.org/10.1029/2021EF002631, 2022.

Patton, N. R., Lohse, K. A., Godsey, S. E., Crosby, B. T., and Seyfried, M. S.: Predicting soil thickness on soil mantled hillslopes, Nat Commun, 9, 3329, https://doi.org/10.1038/s41467-018-05743-y, 2018.

Payton Gardner, W., Susong, D. D., Kip Solomon, D., and Heasler, H.: Snowmelt hydrograph interpretation: Revealing watershed scale hydrologic characteristics of the Yellowstone volcanic plateau, Journal of Hydrology, 383, 209–222, https://doi.org/10.1016/j.jhydrol.2009.12.037, 2010.

Penna, D., Tromp-van Meerveld, H. J., Gobbi, A., Borga, M., and Dalla Fontana, G.: The influence of soil moisture on threshold runoff generation processes in an alpine headwater catchment, Hydrology and Earth System Sciences, 15, 689–702, https://doi.org/10.5194/hess-15-689-2011, 2011.

Prancevic, J. P. and Kirchner, J. W.: Topographic Controls on the Extension and Retraction of Flowing Streams, Geophysical Research Letters, 46, 2084–2092, https://doi.org/10.1029/2018GL081799, 2019.

https://doi.org/10.5194/egusphere-2025-6294
Preprint. Discussion started: 12 January 2026

Prancevic, J. P., Seybold, H., and Kirchner, J. W.: Variability of flowing stream network length across the US, Science, 387, 782–786, https://doi.org/10.1126/science.ado2860, 2025.

Rademacher, L. K., Clark, J. F., Hudson, G. B., Erman, D. C., and Erman, N. A.: Chemical evolution of shallow groundwater as recorded by springs, Sagehen basin; Nevada County, California, Chemical Geology, 179, 37–51, https://doi.org/10.1016/S0009-2541(01)00314-X, 2001.

Rademacher, L. K., Clark, J. F., Clow, D. W., and Hudson, G. B.: Old groundwater influence on stream hydrochemistry and catchment response times in a small Sierra Nevada catchment: Sagehen Creek, California, Water Resources Research, 41, https://doi.org/10.1029/2003WR002805, 2005.

Ridgeway, J. B. and Surfleet, C. G.: Effects of Streamside Buffers on Stream Temperatures Associated With Forest Management and Harvesting Using DHSVM-RBM; South Fork Caspar Creek, California, Front. For. Glob. Change, 4, https://doi.org/10.3389/ffgc.2021.611380, 2021.

Rigge, M. B., Bunde, B., Shi, H., and Postma, K.: Rangeland Condition Monitoring Assessment and Projection (RCMAP) Fractional Component Time-Series Across the Western U.S. 1985-2020 (2.0, October 2021), https://doi.org/10.5066/P95IQ4BT, 2021.

Roberts, M. C. and Archibold, O. W.: Variation of drainage density in a small British Columbia watershed, J American Water Resour Assoc, 14, 470–476, https://doi.org/10.1111/j.1752-1688.1978.tb02183.x, 1978.

Rodhe, A. and Seibert, J.: Groundwater dynamics in a till hillslope: flow directions, gradients and delay, Hydrological Processes, 25, 1899–1909, https://doi.org/10.1002/hyp.7946, 2011.

Sen, P. K.: Estimates of the Regression Coefficient Based on Kendall's Tau, Journal of the American Statistical Association, 63, 1379–1389, https://doi.org/10.1080/01621459.1968.10480934, 1968.

Senatore, A., Micieli, M., Liotti, A., Durighetto, N., Mendicino, G., and Botter, G.: Monitoring and Modeling Drainage Network Contraction and Dry Down in Mediterranean Headwater Catchments, Water Resources Research, 57, e2020WR028741, https://doi.org/10.1029/2020WR028741, 2021.

Shaw, S. B.: Investigating the linkage between streamflow recession rates and channel network contraction in a mesoscale catchment in New York state, Hydrological Processes, 30, 479–492, https://doi.org/10.1002/hyp.10626, 2016.

Soil Survey Staff: Soil Survey Geographic (SSURGO) Database [data set], 2022.

Spence, C.: A Paradigm Shift in Hydrology: Storage Thresholds Across Scales Influence Catchment Runoff Generation, Geography Compass, 4, 819–833, https://doi.org/10.1111/j.1749-8198.2010.00341.x, 2010.

Sproles, E. A., Leibowitz, S. G., Reager, J. T., Wigington, P. J. J., Famiglietti, J. S., and Patil, S. D.: GRACE storage-runoff hystereses reveal the dynamics of regional watersheds, Hydrology and Earth System Sciences, 19, 3253–3272, https://doi.org/10.5194/hess-19-3253-2015, 2015.

Stieglitz, M., Shaman, J., McNamara, J., Engel, V., Shanley, J., and Kling, G. W.: An approach to understanding hydrologic connectivity on the hillslope and the implications for nutrient transport, Global Biogeochemical Cycles, 17, https://doi.org/10.1029/2003GB002041, 2003.

https://doi.org/10.5194/egusphere-2025-6294
Preprint. Discussion started: 12 January 2026

Sun, F., Berg, N., Hall, A., Schwartz, M., and Walton, D.: Understanding End-of-Century Snowpack Changes Over California's Sierra Nevada, Geophysical Research Letters, 46, 933–943, https://doi.org/10.1029/2018GL080362, 2019.

Sun, R., Hernández, F., Liang, X., and Yuan, H.: A Calibration Framework for High-Resolution Hydrological Models Using a Multiresolution and Heterogeneous Strategy, Water Resources Research, 56, e2019WR026541, https://doi.org/10.1029/2019WR026541, 2020.

Tague, C. and Peng, H.: The sensitivity of forest water use to the timing of precipitation and snowmelt recharge in the California Sierra: Implications for a warming climate, Journal of Geophysical Research: Biogeosciences, 118, 875–887, https://doi.org/10.1002/jgrg.20073, 2013.

Thackeray, C. W., Derksen, C., Fletcher, C. G., and Hall, A.: Snow and Climate: Feedbacks, Drivers, and Indices of Change, Curr Clim Change Rep, 5, 322–333, https://doi.org/10.1007/s40641-019-00143-w, 2019.

U.S. Geological Survey: USGS TNM Hydrography (NHD) [data set], 2019.

Venables, W. N. and Ripley, B. D.: Modern Applied Statistics with S, Springer New York, New York, NY, https://doi.org/10.1007/978-0-387-21706-2, 2002.

Von Schiller, D., Bernal, S., Dahm, C. N., and Martí, E.: Nutrient and Organic Matter Dynamics in Intermittent Rivers and Ephemeral Streams, in: Intermittent Rivers and Ephemeral Streams, Elsevier, 135–160, https://doi.org/10.1016/B978-0-12-803835-2.00006-1, 2017.

Ward, A. S., Schmadel, N. M., and Wondzell, S. M.: Simulation of dynamic expansion, contraction, and connectivity in a mountain stream network, Advances in Water Resources, 114, 64–82, https://doi.org/10.1016/j.advwatres.2018.01.018, 2018.

Ward, A. S., Wondzell, S. M., Schmadel, N. M., and Herzog, S. P.: Climate Change Causes River Network Contraction and Disconnection in the H.J. Andrews Experimental Forest, Oregon, USA, Front. Water, 2, https://doi.org/10.3389/frwa.2020.00007, 2020.

Warix, S. R., Navarre-Sitchler, A., Manning, A. H., and Singha, K.: Local Topography and Streambed Hydraulic Conductivity Influence Riparian Groundwater Age and Groundwater-Surface Water Connection, Water Resources Research, 59, e2023WR035044, https://doi.org/10.1029/2023WR035044, 2023.

Whiting, J. A. and Godsey, S. E.: Discontinuous headwater stream networks with stable flowheads, Salmon River basin, Idaho, Hydrological Processes, 30, 2305–2316, https://doi.org/10.1002/hyp.10790, 2016.

Wigmosta, M. S. and Perkins, W. A.: Simulating the Effects of Forest Roads on Watershed Hydrology, in: Land Use and Watersheds: Human Influence on Hydrology and Geomorphology in Urban and Forest Areas, American Geophysical Union (AGU), 127–143, https://doi.org/10.1029/WS002p0127, 2001.

Wigmosta, M. S., Vail, L. W., and Lettenmaier, D. P.: A distributed hydrology-vegetation model for complex terrain, Water Resour. Res., 30, 1665–1679, https://doi.org/10.1029/94WR00436, 1994.

Winter, T. C., Harvey, J. W., Franke, O. L., and Alley, W. M.: Ground water and surface water: A single resource, U.S. Geological Survey, 1999.

https://doi.org/10.5194/egusphere-2025-6294
Preprint. Discussion started: 12 January 2026

Wolfram, S.: Universality and complexity in cellular automata, Physica D: Nonlinear Phenomena, 10, 1–35, https://doi.org/10.1016/0167-2789(84)90245-8, 1984.

Wondzell, S. M.: The role of the hyporheic zone across stream networks, Hydrol. Process., 25, 3525–3532, https://doi.org/10.1002/hyp.8119, 2011.

Zanetti, F., Durighetto, N., Vingiani, F., and Botter, G.: Technical note: Analyzing river network dynamics and the active length–discharge relationship using water presence sensors, Hydrology and Earth System Sciences, 26, 3497–3516, https://doi.org/10.5194/hess-26-3497-2022, 2022.

Zanetti, F., Botter, G., and Camporese, M.: Stream Network Dynamics of Non-Perennial Rivers: Insights From Integrated Surface-Subsurface Hydrological Modeling of Two Virtual Catchments, Water Resources Research, 60, e2023WR035631, https://doi.org/10.1029/2023WR035631, 2024.

Zimmer, M. A. and McGlynn, B. L.: Bidirectional stream–groundwater flow in response to ephemeral and intermittent streamflow and groundwater seasonality, Hydrological Processes, 31, 3871–3880, https://doi.org/10.1002/hyp.11301, 2017a.

Zimmer, M. A. and McGlynn, B. L.: Ephemeral and intermittent runoff generation processes in a low relief, highly weathered catchment, Water Resources Research, 53, 7055–7077, https://doi.org/10.1002/2016WR019742, 2017b.